ICMSM 2024

2nd International Conference on Materials Science and Manufacturing

Editor:
Prof. Dr. Uğur KÖKLÜ

PROCEEDINGS

ISBN: 978-625-94809-5-4

28-29 June | 2024 | Turkey

url: https://matsciman.com

2ND INTERNATIONAL CONFERENCE ON MATERIALS SCIENCE AND MANUFACTURING (ICMSM 2024)
JUNE 28-29, 2024

2. ULUSLARARASI MALZEME BİLİMİ VE İMALAT KONFERANSI (ICMSM 2024)
28-29 HAZİRAN 2024

PROCEEDING E-BOOK/ BİLDİRİLER KİTABI

KARAMAN/TÜRKİYE

COPYRIGHT © 2024

BY ASES CONGRESS ORGANIZATION

PUBLISHING COMPANY LIMITED

ALL RIGHTS RESERVED. NO PART OF THIS PUBLICATION MAY BE REPRODUCED, DISTRIBUTED OR TRANSMITTED IN ANY FORM OR BY ANY MEANS, INCLUDING PHOTOCOPYING, RECORDING OR OTHER ELECTRONIC OR MECHANICAL METHODS, WITHOUT THE PRIOR WRITTEN PERMISSION OF THE PUBLISHER, EXCEPTIN THE CASE OF BRIEF QUOTATIONS EMBODIED IN CRITICAL REVIEWS AND CERTAIN OTHER NONCOMMERCIAL USES PERMITTED BY COPYRIGHT LAW. ASES CONGRESS ORGANIZATION PUBLISHING® IT IS RESPONSIBILITY OF THE AUTHOR TO ABIDE BY THE PUBLISHING ETHICS RULES.

ASES PUBLICATIONS – 2024©

12.07.2024

ISBN: 978-625-94809-5-4

ICMSM 2024
2nd International Conference on Materials Science and Manufacturing

June 28-29, 2024

Online-Live

https://matsciman.com

This conference proceedings book is published as an electronic format as e-book.
Tum Hakları Saklıdır /All Rights Reserved.
* Bu kitapta yazılı olan her türlü bilgi ve yorumun sorumluluğu yazara aittir/ The responsibility for any information and comments written in this book belongs to the authors.
It may not be copied or reproduced without permission.
Temmuz, 2024/ July, 2024

ICMSM 2024

2nd International Conference on Materials Science and Manufacturing

2nd International Conference on Materials Science and Manufacturing (ICMSM 2024), will be held in Turkey during June 28-29, 2024 in online VIRTUAL format.

Conference Topics

- Additive manufacturing
- Biomaterals
- Casting
- Coating
- Composite materials
- Functional materials
- Forming
- Joining
- Labeling and painting
- Manufacturing
- Materials properties
- Materials science and engineering
- Machining
- Mechatronics
- Moulding
- Nano-materials
- New materials
- Shaping processes
- Surface treatment
- Smart materials
- Polymers
- Powder metallurgy
- Production
- Rapid prototyping
- Welding

Important Dates

Abstract Submission Deadline	June 15, 2024
Full Paper Submission Deadline	June 20, 2024
Reviewed Full Paper Submission	June 25, 2024
Registration Deadline	June 25, 2024
Conference Date	June 28-29, 2024

Language: Turkish and English

Conference Website
https://matsciman.com

ASES
ACADEMY OF SCIENTIFIC AND EDUCATIONAL STUDIES

General Information

Genel Bilgi

ICMSM 2024

2nd International Conference on Materials Science and Manufacturing
June 28-29, 2024
Online-Live
https://matsciman.com

Zoom Meeting Information

Please click on the zoom link provided for each session below or the link located in the each session on the program to attend the session of your choice. The Zoom application is free and no need to create an account. Any session can be joined without a password. Meeting passcode will be encrypted and included in the invite link to allow participants to join with just one click without having to enter the passcode. Speakers must be connected to the session 10 minutes before the presentation time.

Technical Information

- Make sure your computer has a microphone and is working.
- You should be able to use screen sharing feature in Zoom.
- Attendance certificates will be sent to you as PDF at the end of the congress.
- Moderator is responsible for the presentation and scientific discussion (question-answer) section of the session.
- Before you login to Zoom please indicate your name surname

exp. NAME SURNAME

Zoom Toplantı Bilgileri

İstediğiniz oturuma katılmak için lütfen aşağıda her oturum için verilen Zoom bağlantısına veya programdaki her oturumda yer alan bağlantıya tıklayın. Zoom uygulaması ücretsizdir ve hesap oluşturmanıza gerek yoktur. Herhangi bir oturuma şifre gerekmeden katılabilirsiniz. Toplantı şifresi şifrelenecek ve katılımcıların şifreyi girmeye gerek kalmadan tek tıklamayla toplantıya katılmasına olanak sağlamak için davet bağlantısına eklenecek. Konuşmacıların sunum saatinden 10 dakika önce oturuma bağlanması gerekmektedir. Tüm kongre katılımcıları canlı bağlanarak tüm oturumları dinleyebilir.

Teknik Bilgiler

- Bilgisayarınızda mikrofon olduğuna ve çalıştığına emin olun.
- Zoom'da ekran paylaşma özelliğine kullanabilmelisiniz.
- Katılım belgeleri kongre sonunda tarafınıza PDF olarak gönderilecektir.
- Moderatör – oturumdaki sunum ve bilimsel tartışma (soru-cevap) kısmından sorumludur.
- Zoom'a giriş yapmadan önce lütfen adınızı soyadınızı belirtiniz. Örnek: AD SOYAD

Communication

İletişim

Principal Contact
E-mail: kongre@matsciman.com
Web page: https://matsciman.com

ICMSM 2024 2nd International Conference on Materials Science and Manufacturing
June 28-29, 2024-Turkey

ICMSM 2024

2nd International Conference on Materials Science and Manufacturing
June 28-29, 2024
Online-Live
https://matsciman.com

Moderating a Session

We appreciate all of the moderators' contributions to the conference. The moderators are expected to assist us in the smooth functioning of the conference.

- ❖ Please keep in mind that each presenter has a total of 20 minutes. It's important to have perfect timing.
- ❖ The moderator decides whether to take questions from the audience: at the end of each presentation or at the end of the session.
- ❖ Please remind attendees to send their questions and comments to the Zoom chat.
- ❖ Finally, if any of the presenters in your session does not participate and present her/his paper, please notify us by sending an email to kongre@matsciman.com.

Presentation Information

Each presentation has a **total time limit of 20 minutes**: 15 minutes for the presentation + 5 minutes for questions & answers. The moderator has the authority to rearrange the presentation order in the session. Please arrive at least 5 minutes prior to the start of your session and turn on your camera during your presentation. Please keep in mind that each presenter is required to remain for the duration of the session.

ICMSM 2024

2nd International Conference on Materials Science and Manufacturing

June 28-29, 2024

Online-Live

https://matsciman.com

Committees

Komiteler

Organizing Committee

- Aamer Sharif, Ph.D, Cecos University of IT and Emerging Science, Pakistan.
- Daniel Chuchala, Ph.D, Gdansk University of Technology Poland.
- Ekrem Oezkaya, Ph.D, Institute of Machining Technology, TU Dortmund, Germany.
- Eva Schmidova, Ph.D, University of Pardubice, Czech Republic.
- Fuat Kara, Ph.D, Düzce University, Türkiye.
- Gururaj Bolar, Ph.D, Manipal Academy of Higher Education, India.
- Khaled Giasin, Ph.D, University of Portsmouth, United Kingdom.
- Muhammad Faisal, PhD. Allama Iqbal Open University, Pakistan
- Uğur Köklü, Ph.D, Karamanoğlu Mehmetbey University, Turkey (Conference Chairman)

*Listed alphabetical order by name

Science Committee

- A.Tamilarasan, PhD. Er.Perumal Manimekalai Engineering College, India.
- Engin Kocaman, PhD. Zonguldak Bulent Ecevit University, Turkey.
- Erkin Akdoğan, PhD, Karamanoğlu Mehmetbey University, Turkey.
- Grzegorz M. Królczyk, PhD, Opole University of Technology, Poland.
- Hüsnü Gerengi, PhD, Duzce University, Turkey.
- Ionut Cristian SCURTU, PhD. Eng., Naval Academy Constanta Romania
- Levent Urtekin, PhD, Kırşehir Ahi Evran University, Turkey.
- LokeshK Sri Ramamurth, PhD, Srinivas Institute of Technology, India.
- Mahmoud Khedr, PhD, Benha University, Egypt.
- Mitsuo Niinomi, PhD, Tohoku University, Japan.
- Mohamed A. Eltaher, PhD. King Abdulaziz University, Saudi Arabia.
- Muhammad Faisal, PhD. Allama Iqbal Open University, Pakistan
- Muhammad Pervej Jahan, PhD. Miami University, United States
- Murat Sarıkaya, PhD, Sinop University, Turkey.
- Mustafa Kuntoğlu, PhD, Selçuk University, Turkey.
- Oğuz Koçar, PhD. Zonguldak Bulent Ecevit University, Turkey.
- Shujian Li, PhD, Hunan University of Science and Technology, China.
- Şakir Yazman, PhD, Selçuk University, Turkey.

*Listed alphabetical order by name

ICMSM 2024 2nd International Conference on Materials Science and Manufacturing
June 28-29, 2024-Turkey

From the President of the Conference,

Greetings to all participants,

It is a great pleasure for me to welcome you to the 2nd International Conference on Materials Science and Manufacturing (ICMSM) 2024 Conference.

We hope that this conference will create a friendly occasion for all to share perspectives and research findings from a wide variety of all engineering. We also dearly value possible friendships and partnerships made and insights gained at the conference and hope they will go beyond your participation in the conference, leading to better understanding and appreciation of our profession from an international stance.

With very best wishes,

Prof. Dr. Uğur KÖKLÜ

President of ICMSM 2024

Açılış Konuşması

Değerli katılımcılar Uluslararası Malzeme Bilimi ve İmalat konferans başkanı olarak sizleri en kalbi duygularımla selamlıyorum ve konferansımıza hoş geldiniz diyorum. Değerli katılımcılar davetimizi dikkate alarak Uluslararası Malzeme Bilimi ve İmalat Konferansına bildiri ile katılım sağladığınız için çok teşekkür ederiz. Uluslararası Malzeme Bilimi ve İmalat Konferansı çevrimiçi olarak gerçekleştirilecektir. Konferans, malzeme bilimi ve imalat alanındaki teknolojik gelişmeleri ve araştırma sonuçlarını sunmak ve paylaşmak için uluslararası bir platform görevi görecektir. Sanal ortamda dahi olsa sizleri ağırlamaktan ve bilgi paylaşımından dolayı çok mutlu oluyoruz. Umut ediyoruz ki sizlerle verimli ve unutulmaz bir konferans yaşayacağız. Konferansta toplam 12 bildiri sunulacaktır. Türkiye, İspanya, Romanya ve Hindistan'dan bilim insanlarının yer aldığı bildiriler sunulacaktır. Konferansımızda hem endüstriden hem de akademik camiadan bildiriler bulunmaktadır. Umut ediyorum ki arzulanan Üniversite ile endüstri bir araya gelerek çok başarılı çalışmalar yapılacaktır. Konferansta 3 oturum olacaktır. Bir sonraki konferansta görüşmek temennisiyle

Konferansımıza katıldığınız için tekrar teşekkür ederim.

Saygılarımla

Programme

Program

Friday, June 28, 2024 Time zone in Turkey (UTC+3)	**28 Haziran Cuma** 2024
Meeting ID: 269 738 6033 Password: 34abcd https://us06web.zoom.us/j/83330427285?pwd=SEpd0hCZIxllKF2wB7rnYV97PySxb4.1 Click to connect/bağlanmak için tıklayınız	
Opening speech/Açılış konuşması	
09:10-09:20 AM	**Dr. Uğur Köklü**, Conference Chairman
Session 1	**(09:20-10:40 AM)** **Session Chair: Dr. Şakir YAZMAN**
09:20-09:40 AM	Özel Kafa Altı Puntalı Kaynak Formlu Perçin Tasarımı ve Simülasyon Destekli Üretimi Aslıhan KALYON, Alper BAYGUT, Yener YILMAZ, Furkan BELLİBAŞ
09:40-10:00 AM	Software Approaches And Metallurgical Characterization in the Casting Production of 2-Piece Ball Valves Sezer Hivda ÖZDEN, Ozan ÇOBAN
10:00-10:20 AM	Busbar Enerji Dağıtım Sistemi Elektrik Simülasyonları Ahmet Can YALÇIN, Mehmet Can BÜYÜKDÖĞERLİOĞLU, Hıdır GÖGÜLTER, Vedat VOŞKİ, Dursun ERİŞ, Tunahan İNAT, Ahmet FEYZİOĞLU
10:20-10:40 AM	Savunma Sanayinde Zırh, Koruma ve Görünmezlik Teknolojileri Almıla Gökçe DAL, İzel YUMAK
10:40 AM-02:00 PM Break	

Session 2	**(02:00-04:00 PM)** **Session Chair: Dr. Mehmet ŞAHBAZ**
02:00-02:20 PM	Seçici lazer ergitme yöntemi ile üretilen alsi10mg alaşımların kriyojenik işlemi Pelin SEZER, Semra KURAMA Taner KARAGÖZ
02:20-02:40 PM	Investigatin of Microstructure and Mechanical Properties of Cuconibe Alloy Formed by Rollıng and Forging Method Feyzanur Öztürk, Volkan Karakurt, Talip Çitrak, Feriha Birol, Orçun Zığındere
02:40-03:00 PM	Dimensional Behavior Comparison of Injection Molded PA-6 AND PA-66 Meltem UZUNOĞLU, Harun ZENGİN
03:00-03:20 PM	Comparative Mechanical and Electrochemical Behaviour of Dissimilar Friction Stir Welded AA6082 and AA2014 Weldments K T Thilagham, D Noorullah
03:20-03:40 PM	Mycoremediation of Heavy Metal Pollution: A Review Cazan Bogdan, Iordache Ovidiu-George, Mihai Carmen, Perdum Elena, Dinca Laurentiu
03:40-04:00 PM	Ganoderma Lucidum Leather as a Sustainable Alternative Potential for Fashion Industry Cazan Bogdan, Iordache Ovidiu-George, Mihai Carmen, Perdum Elena, Dinca Laurentiu
04:00 PM Break	

Saturday, June 29, 2024 Time zone in Turkey (UTC+3)	**29 Haziran Cumartesi** 2024
Meeting ID: 269 738 6033 Password: 34abcd https://us06web.zoom.us/j/83330427285?pwd=SEpd0hCZIxllKF2wB7rnYV97PySxb4.1 Click to connect/bağlanmak için tıklayınız	
Session 3	**(10:20-11:00 AM)** **Session Chair: Dr. Sezer Morkavuk**
10:20-10:40 AM	Roughness and Microstructure Characterization of AISI 316l Laser-Powder Bed Fusion Specimens After Applying a Vibration -Assisted Ball Burnishing Process Eric Velázquez-Corral, Adrián Travieso-Disotuar, Ramón Jerez-Mesa, Montserrat Vilaseca, Clément Keller and Gilles Dessein
10:40-11:00 AM	Influence of Printing Parameters in the Inter-Layer Bonds Formation in Thermoplastic Polyurethane Walter Crupano, Bàrbara Adrover-Monserrat, Jordi Llumà, J. Antonio Travieso-Rodriguez

PROCEEDINGS / BİLDİRİLER

TAM METİN SUNUMLAR

INFLUENCE OF PRINTING PARAMETERS IN THE INTER-LAYER BONDS FORMATION IN THERMOPLASTIC POLYURETHANE

Walter CRUPANO[1], Bàrbara ADROVER-MONSERRAT[2], Jordi LLUMÀ[3], J. Antonio TRAVIESO-RODRIGUEZ[4]

[1]Universitat Politècnica de Catalunya, Escola d'Enginyeria de Barcelona Est, Mechanical Engineering Department, walter.crupano@upc.edu
[2] Universitat Politècnica de Catalunya, Escola d'Enginyeria de Barcelona Est, Mechanical Engineering Department, barbara.adrover@upc.edu
[3] Universitat Politècnica de Catalunya, Escola d'Enginyeria de Barcelona Est, Materials Science and Metallurgical Engineering Department, jordi.lluma@upc.edu
[4] Universitat Politècnica de Catalunya, Escola d'Enginyeria de Barcelona Est, Mechanical Engineering Department, antonio.travieso@upc.edu

Abstract
Thermoplastic polyurethane (TPU) is a copolymer that has high flexibility together with good mechanical properties. These advantages are used to manufacture parts through 3D printing for applications in different industrial areas such as biomedicine. Focusing particularly on the technique of Material Extrusion (MEX), this paper studies the influence of the printing parameters on the quality of the inter-layer bonds created with a TPU. The study was conducted to address the challenge of printing vertical walls without supports and in various orientations. The goal was to manufacture a surface that met design restrictions requested by a partner outside the research group. To quantify the quality of the bonds, the mechanical behavior of the tensile tested samples is assessed following the ASTM D638-IV standard. For this purpose, samples were manufactured according to a complete factorial design of experiments. The printing orientation, the wall thickness, and the printing velocity were considered variable parameters. The Young's modulus, the elastic limit and the maximum stress, were measured in each of the tested specimens. Subsequently, the statistical influence of the parameters on each of the measured properties was evaluated, through an analysis of variance. The results showed that the studied parameters have a certain influence on the bonds between layers, but not all of them have an effect on the same measured properties. In general, the printing orientation is the parameter that has shown the most statistical influence and, on the contrary, the printing velocity the least. A second-order analysis concluded that there are also interactions between some parameters that show a statistically significant influence. Specifically, the interaction of printing orientation with wall thickness had the highest influence. It has been concluded that the best bonds between layers are obtained in printed pieces oriented at 90º, at 25 mm/s velocity, and with 0.8 mm wall thickness.

***Keywords*:** Additive manufacturing, material extrusion, tensile tests, inter-layer bonding.

INTRODUCTION

Additive manufacturing (AM) is a set of part manufacturing techniques based on the construction of objects layer by layer. The rapid evolution achieved in recent years demonstrates the potential of AM to prevail in the finite products market [1]. These manufacturing techniques revolutionize the common subtractive process, reducing the need for tooling, while providing a certain flexibility in the design of

the parts [2]. The result of AM techniques is an integration of the design stage into the manufacturing stage. Although AM is used with low production volumes, due to the limitation of the process itself, it allows frequent modifications to the design and offers customization of the final product [3,4]. The typical processes of AM techniques are summarized in the ASTM 52900 standard. One these techniques is material extrusion (MEX), previously called fused filament fabrication (FFF) or fused deposition modeling (FDM). After Scott Crump patented this manufacturing process in 1989, it became the most popular technique [5,6]. The different names used for this extrusion technique are some of those accepted in the literature to refer to a low-cost process that uses filaments to generate complex geometries [7].

The materials used in the MEX process are thermoplastic polymers that, sufficiently heated by an extruder, are deposited on a heated bed progressively, building the designed object. They are usually reinforced with natural fibers or another polymer to improve their performance [8]. The range of polymers available on the market goes from thermoplastics such as polylactic acid (PLA), characterized by its high rigidity and mechanical resistance, to thermoplastic elastomeric (TPE), which stand out for their flexibility and ability to withstand large deformations [9]. Elastomeric filaments that are well suited to MEX have a low glass transition temperature (Tg) associated with a high crystallization rate, but are generally amorphous and are supplied above the Tg [10]. In opposition, TPE are a family of polymers with wide industrial applications. However, they present difficulties when printed by MEX [11]. Researchers generally improve these difficulties by controlling the different printing parameters [12–16].

Within the TPE, thermoplastic polyurethanes (TPU) have characteristics similar to elastomers and are capable of providing a behavior similar to rubber even if they are 3D printed [17]. The elastic behavior of TPU fits perfectly into the MEX process [18]. TPUs are copolymers formed by soft segments (SS) and hard segments (HS), which allow them to exhibit a combination of resistance and flexibility[19,20]. They can have a variable Shore A hardness, depending on the SS and HS content, as well as their chemical structures [21,22]. These materials are widely used in different areas such as biomedical products, electronic devices, automotive components, and textiles [23,24]. Emami et al. [25] demonstrated the potential of TPU for the manufacture of complex geometries such as 3D-printed flexible molds. Gonzalez et al. [21] used the TPU manufactured through the MEX technique to produce dielectric devices, testing its properties in these type of structures. Katschnig et al. [26] explored the use of TPU in biofunctional maxillofacial implants. The research positively assessed the biological compatibility of the TPU/PETG hybrid manufactured by MEX as suitable for personalized implants in the maxillofacial area. Overall, it is demonstrated that TPU is an interesting material for many different actual applications. However, their final performance when 3D-printed depends on the selected parameters used in the slice of the samples.

The correlation between manufacturing by MEX and the properties of the product is complex and in great measure, depending on the union between the deposited filaments and layers. Previous studies show that these bonds are related to printing parameters and influence mechanical [27–29]. Kasmi et al. [30] determined that increasing the speed from 15 mm/s to 100 mm/s caused a reduction in the tensile strength of the TPU. In fact, high printing speeds cause defects due to non-constant flow [31]. In order to optimize the MEX process, Lin at al.[10] related the printing velocity with the mechanical properties using TPU with different hardness. They determined that to obtain better resistance, the velocity must be regulated depending on the filament hardness. Arifvianto et al. [32] showed that the bidirectional configuration of TPU processed by MEX does not improve its mechanical properties. Other authors evaluated the union of the fused filaments, concluding that the printing temperature is influential for the bonds between filaments [33,34]. Striemann et al. [34] improved the bonds between layers through in situ infrared heating. In fact, the study by Gumus et al. [35] analyzed a temperature range of 170-250ºC,

and revealed that the increase in temperature favors the adhesion between layers. In addition, they found that adequate adhesion between layers is obtained by regulating the printing bed temperature. Spoerk et al. [36] suggest keeping the bed at a temperature around the glass transition temperature of the material used. Layer height is another printing parameter that determines different mechanical responses. In fact, it influences the width of the spaces created between the filaments [37]. Garg et al. [38] addressed the problem of dimensional precision tied to the MEX process and analyzed layer height, infill density, and printing velocity. The study concluded that layer height is the most determining factor of those analyzed.

The anisotropic characteristics revealed in MEX printed pieces are a result of difficult bonds between the deposited layers, according to Gao et al.[39]. Beyond the analyzed literature, the importance of the relation between printing parameters and the mechanical behavior of printed pieces remains to be demonstrated. However, it is clear that the bonds between layers play an important role in this mechanism [33,34,40,41]. In order to go deeper on this topic, the present paper aims to study the quality of adhesion generated between layers in TPU parts manufactured by MEX, known as inter-layer bonds. This study is valuable because, on the one hand, MEX is a suitable technique for manufacturing pieces using polymeric filaments and, on the other hand, it also has some extruding compatibility limitations when soft materials such as TPU are used. Furthermore, if MEX technique users are able to achieve good quality of bonds created between layers, they will also achieve good mechanical properties. This problem concerns most of the 3D printing processes.

MATERIAL AND METHODS

As it has been demonstrated in the introduction, the bonds created by the deposited filaments determine the performance of the final pieces. Therefore, it is necessary to analyze the quality of parts manufactured through vertical walls with different angles of inclination, without using supports. This Design of Experiments (DoE) emerges from a demand from a company, as they need to print as in the part shown in Figure 1-a. Thus, the objective is to find the best manufacturing parameters using the different inclination angles shown in Figure 1-a. Therefore, the best inter-layer bonds (Figure 1-b) will be found, increasing the quality of parts.

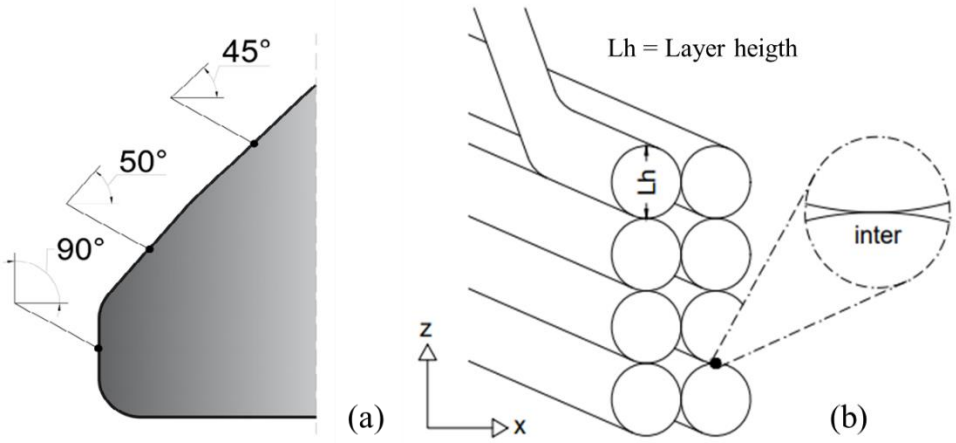

Figure 1. (a) Orientation of the analyzed walls. (b) Diagram of the deposited filaments focalizing the inter-layer formation [42].

To do that, a DoE technique was used. Three printing parameters are chosen as variables: printing orientation, wall thickness, and printing velocity. The orientation defines the inclination in which the part is printed and it determines different mechanical characteristics. The wall thickness defines the number

of intra-layer bonds that are generated in each layer. Velocity is the parameter that determines the speed at which the extruder moves. It generally has an impact on printing time and the quality of inter-layer adhesion.

The material used in this work is a filament of TPU 98A in a 1.75 mm diameter, classified as semi-flexible material. It offers high tensile strength and high elongation at break values [43,44]. It is manufactured by Fillamentum Company from Czech Republic.

The specimens have been printed at 240 ºC and a layer height of 0.2 mm with configurations that consider the three angles determined in Figure 1-a (45º, 50º, 90º) and two wall thicknesses (0.8 and 3.2 mm). Moreover, the velocity was studied at two different levels (25 and 40 mm/s). Table 1 compiles the selected full factorial DoE used, as well as, the different considered configurations. Three repetitions of each configuration were reproduced. The combination of a wall thickness of 3.2 mm with a velocity of 40mm/s was discarded due to printing difficulties.

Table 1. Factors and their levels considered on the DoE.

Factor	Levels	Values
Orientation	3	45 50 90
Wall thickness	2	0.8 3.2
Velocity	2	25 40

The samples follow the ASTM D638-IV standard and were modeled with SolidWorks software. They were manufactured using a Creality Ender 3 printer (Shenzhen Creality 3D Technology Co., Ltd., Guangdong, China), following the printing configurations chosen for this TPU. Subsequently, the specimens were subjected to a tensile test, using a Zwick Roell Z005 universal testing machine, at a 5 mm/s testing speed and a maximum load of 4500 N. The results of the tensile test were compiled in a TestXpert software associated with the universal machine. The specimen's geometry and the experimental setup are shown in Figure 2-a and Figure 2-b.

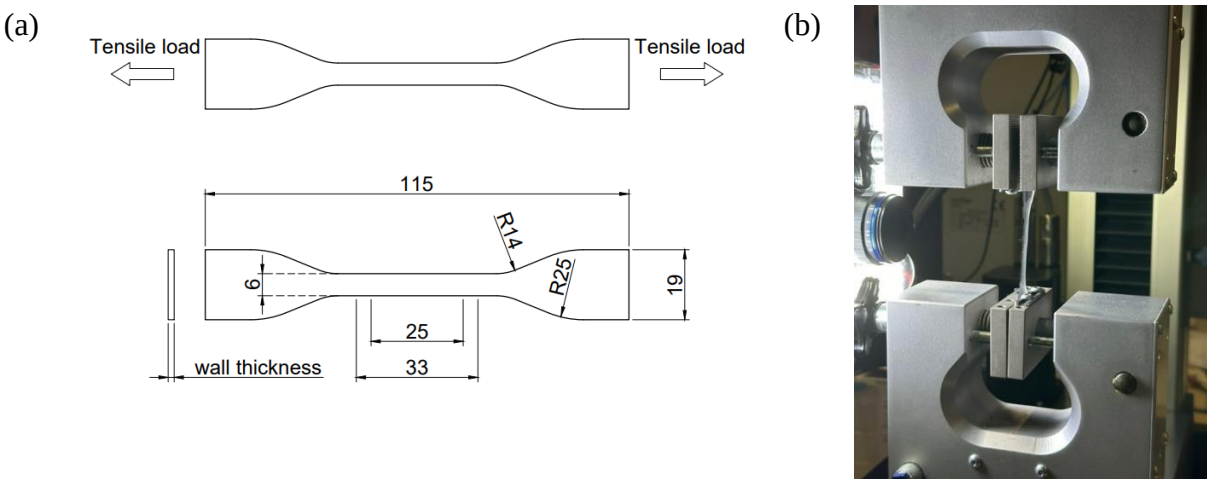

Figure 2. (a) Test specimens ASTM D638-IV (measures in millimeters). (b) Universal Testing Machine.

To analyze the effect of the printing parameters on the mechanical response, an analysis of variance (ANOVA) was performed. The associated p-value was determined considering a significant level of 95% ($\alpha = 0.05$), which allowed us to observe whether the printing parameters significantly influenced the

mechanical response. The parameters obtained in the tensile tests considering the means of the three samples tested and their respective deviations are shown in Table 2.

RESULT AND DISCUSSION

Table 2 shows the mechanical response analyzed (Young's Modulus, E; yield strength, $Rp_{0.2}$; and maximum strength, S_{max}) according to the manufacturing parameters studied.

Table 2. Results and deviations of the different configurations.

Printing parameters				Tensile results		
Combi-nation	Orientation [º]	Velocity [mm/s]	Wall thickness [mm]	E [MPa]	$Rp_{0.2}$ [MPa]	Smax [MPa]
1	45	25	0.8	221.6 ± 23.9	1.48 ± 0.13	15.9 ± 8.55
2	45	40	0.8	143.9 ± 4.03	0.96 ± 0.03	12.9 ± 2.71
3	45	25	3.2	204.7 ± 59.1	1.28 ± 0.39	9.84 ± 8.04
4	50	25	0.8	257.8 ± 6.62	1.65 ± 0.03	23.1 ± 0.79
5	50	40	0.8	239.8 ± 16.6	1.63 ± 0.06	18.3 ± 2.02
6	50	25	3.2	148.3 ± 6.38	0.89 ± 0.07	3.55 ± 2.22
7	90	25	0.8	268.8 ± 6.73	1.69 ± 0.01	18.9 ± 0.31
8	90	40	0.8	266.9 ± 9.96	1.66 ± 0.11	20.7 ± 0.26
9	90	25	3.2	196.3 ± 34.8	1.22 ± 0.21	6.97 ± 1.10

The influence of the printing parameters and their interactions are shown in Table 3. The results of the ANOVA show that the wall thickness is the only influential parameter for all the mechanical properties under study since their associated p-values are lower at 0.05. The other parameters are not statistically influential even though for the Young's Modulus the orientation is at the limit of influence. In fact, the 90º orientation has a maximum Young's modulus of 243.95 MPa, with a steeper slope between 50º and 90º, compared to the lope between 45º and 50º (Figure 3). The combination of 90º with the lowest printing speed (25 mm/s) produces the highest mechanical response. In this case, the values obtained are 266.9 MPa for Young's modulus and 1.69 MPa for yield strength.

The 0.8 mm level guarantees a good mechanical response. Both in the elastic and plastic behavior zone, the highest S_{max} values are obtained in the printed parts with 0.8 mm walls, suggesting better adhesion between filaments when the wall thickness is lower.

Furthermore, it is observed that no interaction between manufacturing parameters considered in this study is statistically influential for the studied mechanical properties.

Table 3. P-values obtained in Minitab for mechanical parameters.

Factor	**p-value**

	E [Mpa]	**Rp0.2** [Mpa]	**Smax** [Mpa]
Orientation	0.055	0.089	0.615
Velocity	0.091	0.102	0.444
Wall thickness	0.002	0.000	0.000
Orientation*Wall thickness	0.225	0.134	0.563
Orientation*Velocity	0.140	0.147	0.122

Figure 3 shows the effects of the printing parameters in the tensile tests for Young's modulus and the yield strength (parameters that define the elastic behavior zone).

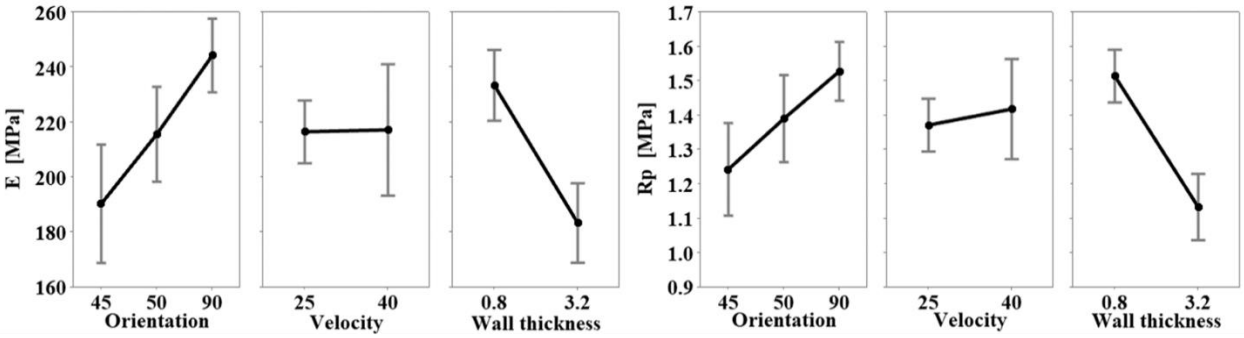

Figure 3. Main effect plots for Young modulus and yield strength.

The main effects plots for maximum stress are shown in Figure 4. As evident, the 90º print orientation and 0.8 mm wall thickness give the best results. Moreover, although speed is not influential, the best responses are obtained at 40 mm/s.

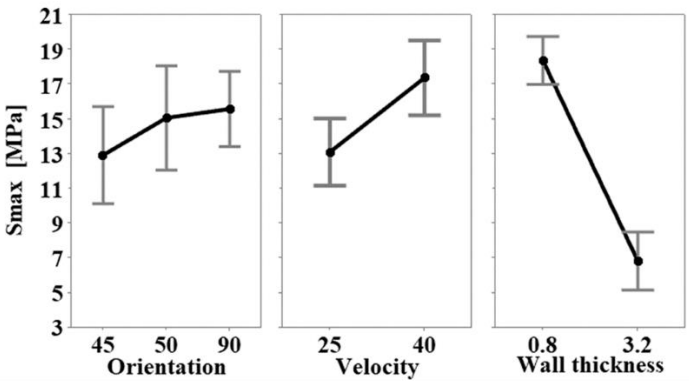

Figure 4. Main effect plot for maximum stress.

Analyzing the results obtained, the configuration that offers the highest strength is in the sample printed at 50º, at 25 mm/s speed, with a wall thickness of 0.8 mm; with a S_{max} value of 21.08 MPa.
Figure 5 shows the Stress-strain curve of this same configuration.

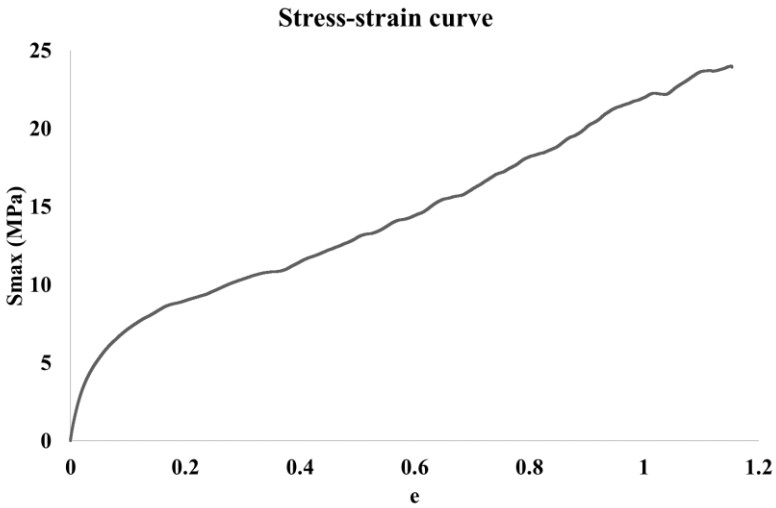

Figure 5. Stress-strain curve with a configuration of 50º, 25 mm/s, 0.8 mm.

However, Young's modulus and the yield strength reach a maximum value in the printed part at 90º, 25 mm/s speed, and 0.8 mm wall thickness, obtaining a S_{max} of 18.91 MPa. In the present study, the vertical orientation represents the best condition to generate good interlayer adhesions. In fact, the literature confirms the 90º orientation as a necessary condition for good resistance [32].
Besides, in the elastic zone, comparable values are achieved with configurations 7 and 8, both with a 90º orientation and a wall thickness of 0.8 mm. It is shown that the thickness influences the adhesion between filaments and can control the formation of voids [45]. The typical anisotropy of samples printed in MEX is a documented condition related to printing parameters [46]. Poor adhesion between filaments causes voids that reduce the mechanical performance of printed parts [47]. Although this research provides a relationship between adhesion between deposited filaments and printing parameters, it paves the way for future studies.

CONCLUSIONS

The use of the MEX technique to manufacture parts using flexible polymers such as TPU is not yet fully documented, especially the mechanical characterization of the parts obtained. This study has delved into the relationship between the printing parameters to be used and the mechanical behavior by analyzing the cohesion of different layers.

The results obtained showed that the wall thickness influences in terms of maximum stress. In particular, good inter-layer bonds are formed in the vertical orientation and wall thickness of 0.8 mm, determining a dependence of the inter-layer bonds on the orientation. From this study it can be concluded that the supports are dispensable with printing angles greater than 45º, also guaranteeing good unions between filaments.

The mechanical properties obtained in the parts printed by MEX with TPU make it usable for different industrial applications, specifically for the one that was being evaluated in the biomedical sector.

REFERENCES

[1] G. Prashar, H. Vasudev, D. Bhuddhi, Additive manufacturing: expanding 3D printing horizon in industry 4.0, Int. J. Interact. Des. Manuf. (2022). https://doi.org/10.1007/s12008-022-00956-4.

[2] I. Gibson, D. Rosen, B. Stucker, M. Khorasani, Additive Manufacturing Technologies, 2020.

[3] M. Jiménez, L. Romero, I.A. Domínguez, M.D.M. Espinosa, M. Domínguez, Additive Manufacturing Technologies: An Overview about 3D Printing Methods and Future Prospects, Complexity 2019 (2019). https://doi.org/10.1155/2019/9656938.

[4] V. Dhinakaran, K.P.M. Kumar, P.M.B. Ram, M. Ravichandran, M. Vinayagamoorthy, A review on recent advancements in fused deposition modeling, Mater. Today Proc. 27 (2020) 752–756. https://doi.org/10.1016/j.matpr.2019.12.036.

[5] J.R.C. Dizon, A.H. Espera, Q. Chen, R.C. Advincula, Mechanical characterization of 3D-printed polymers, Addit. Manuf. 20 (2018) 44–67. https://doi.org/10.1016/j.addma.2017.12.002.

[6] S.C. Altıparmak, V.A. Yardley, Z. Shi, J. Lin, Extrusion-based additive manufacturing technologies: State of the art and future perspectives, J. Manuf. Process. 83 (2022) 607–636. https://doi.org/10.1016/j.jmapro.2022.09.032.

[7] G.D. Goh, Y.L. Yap, H.K.J. Tan, S.L. Sing, G.L. Goh, W.Y. Yeong, Process–Structure–Properties in Polymer Additive Manufacturing via Material Extrusion: A Review, Crit. Rev. Solid State Mater. Sci. 45 (2020) 113–133. https://doi.org/10.1080/10408436.2018.1549977.

[8] L.J. Tan, W. Zhu, K. Zhou, Recent Progress on Polymer Materials for Additive Manufacturing, Adv. Funct. Mater. 30 (2020) 1–54. https://doi.org/10.1002/adfm.202003062.

[9] L. Musa, N. Krishna Kumar, S.Z. Abd Rahim, M.S. Mohamad Rasidi, A.E. Watson Rennie, R. Rahman, A. Yousefi Kanani, A.A. Azmi, A review on the potential of polylactic acid based thermoplastic elastomer as filament material for fused deposition modelling, J. Mater. Res. Technol. 20 (2022) 2841–2858. https://doi.org/10.1016/j.jmrt.2022.08.057.

[10] X. Lin, P. Coates, M. Hebda, R. Wang, Y. Lu, L. Zhang, Experimental analysis of the tensile property of FFF-printed elastomers, Polym. Test. 90 (2020) 106687. https://doi.org/10.1016/j.polymertesting.2020.106687.

[11] P. Awasthi, S.S. Banerjee, Fused deposition modeling of thermoplastic elastomeric materials: Challenges and opportunities, Addit. Manuf. 46 (2021) 102177. https://doi.org/10.1016/j.addma.2021.102177.

[12] N. Verma, P. Awasthi, P.M. Pandey, S.S. Banerjee, Development of material extrusion 3D printing compatible tailorable thermoplastic elastomeric materials from acrylonitrile butadiene styrene and styrene-(ethylene-butylene)-styrene block copolymer blends, J. Appl. Polym. Sci. (2022) 1–15. https://doi.org/10.1002/app.53039.

[13] J. Suder, J. Mlotek, A. Panec, F. Fojtík, Design of Printing Parameter Settings Methodology for FFF Printing of Waterproof Samples from a Flexible Material, Acta Mech. Slovaca 27 (2023) 58–64. https://doi.org/10.21496/ams.2023.017.

[14] D. Chaidas, J.D. Kechagias, An investigation of PLA/W parts quality fabricated by FFF, Mater.

Manuf. Process. 37 (2022) 582–590. https://doi.org/10.1080/10426914.2021.1944193.

[15] A. Tayeb, J.B. Le Cam, B. Loez, 3D printing of soft thermoplastic elastomers: Effect of the deposit angle on mechanical and thermo-mechanical properties, Mech. Mater. 165 (2022) 104155. https://doi.org/10.1016/j.mechmat.2021.104155.

[16] I. Koutsamanis, A. Paudel, C.P. Alva Zúñiga, L. Wiltschko, M. Spoerk, Novel polyester-based thermoplastic elastomers for 3D-printed long-acting drug delivery applications, J. Control. Release 335 (2021) 290–305. https://doi.org/10.1016/j.jconrel.2021.05.030.

[17] W. Michaeli, R. Heinz, Foam extrusion of thermoplastic polyurethanes (TPU) using CO2 as a blowing agent, Macromol. Mater. Eng. 284–285 (2000) 35–39. https://doi.org/10.1002/1439-2054(20001201)284:1<35::AID-MAME35>3.3.CO;2-3.

[18] S.M. Desai, R.Y. Sonawane, A.P. More, Thermoplastic polyurethane for three-dimensional printing applications: A review, Polym. Adv. Technol. 34 (2023) 2061–2082. https://doi.org/10.1002/pat.6041.

[19] J. Xu, L. Cheng, Z. Zhang, L. Zhang, C. Xiong, W. Huang, Y. Xie, L. Yang, Highly exfoliated montmorillonite clay reinforced thermoplastic polyurethane elastomer:: In situ preparation and efficient strengthening, RSC Adv. 9 (2019) 8184–8196. https://doi.org/10.1039/c8ra10121c.

[20] N. Hossieny, V. Shaayegan, A. Ameli, M. Saniei, C.B. Park, Characterization of hard-segment crystalline phase of thermoplastic polyurethane in the presence of butane and glycerol monosterate and its impact on mechanical property and microcellular morphology, Polymer (Guildf). 112 (2017) 208–218. https://doi.org/10.1016/j.polymer.2017.02.015.

[21] D. Gonzalez, J. Garcia, B. Newell, Electromechanical characterization of a 3D printed dielectric material for dielectric electroactive polymer actuators, Sensors Actuators, A Phys. 297 (2019) 111565. https://doi.org/10.1016/j.sna.2019.111565.

[22] N. Elmrabet, P. Siegkas, Dimensional considerations on the mechanical properties of 3D printed polymer parts, Polym. Test. 90 (2020) 106656. https://doi.org/10.1016/j.polymertesting.2020.106656.

[23] H.Y. Mi, X. Jing, J. Peng, L.S. Turng, X.F. Peng, Influence and prediction of processing parameters on the properties of microcellular injection molded thermoplastic polyurethane based on an orthogonal array test, J. Cell. Plast. 49 (2013) 439–458. https://doi.org/10.1177/0021955X13488399.

[24] H. Lee, R.I. Eom, Y. Lee, Evaluation of the mechanical properties of porous thermoplastic polyurethane obtained by 3D printing for protective gear, Adv. Mater. Sci. Eng. 2019 (2019). https://doi.org/10.1155/2019/5838361.

[25] N. Emami, Employing additive manufacturing to create reusable TPU formworks for casting topologically optimized facade panels, J. Build. Eng. 75 (2023) 106946. https://doi.org/10.1016/j.jobe.2023.106946.

[26] M. Katschnig, J. Wallner, T. Janics, C. Burgstaller, W. Zemann, C. Holzer, Biofunctional glycol-modified polyethylene terephthalate and thermoplastic polyurethane implants by extrusion-based additive manufacturing for medical 3D maxillofacial defect reconstruction, Polymers (Basel). 12

(2020). https://doi.org/10.3390/POLYM12081751.

[27] N. Vidakis, M. Petousis, A. Korlos, E. Velidakis, N. Mountakis, C. Charou, A. Myftari, Strain rate sensitivity of polycarbonate and thermoplastic polyurethane for various 3d printing temperatures and layer heights, Polymers (Basel). 13 (2021). https://doi.org/10.3390/polym13162752.

[28] D.H. Abang Ismawi Hassim, N.I. Nik Ismail, S.S. Sarkawi, Y.W. Ngeow, S. Ibrahim, K.C. Yong, The feasibility of using ethylene-vinyl acetate/natural rubber (EVA/NR)-based thermoplastic elastomer as filament material in fused deposition modelling (FDM)-3D printing application, J. Rubber Res. 24 (2021) 659–668. https://doi.org/10.1007/s42464-021-00145-0.

[29] E.O. Bachtiar, O. Erol, M. Millrod, R. Tao, D.H. Gracias, H. Romer, S. Hoon, Journal of the Mechanical Behavior of Biomedical Materials 3D printing and characterization of a soft and biostable elastomer with high flexibility and strength for biomedical applications, J. Mech. Behav. Biomed. Mater. 104 (2020) 103649. https://doi.org/10.1016/j.jmbbm.2020.103649.

[30] S. Kasmi, G. Ginoux, E. Labbé, S. Alix, Multi-physics properties of thermoplastic polyurethane at various fused filament fabrication parameters, Rapid Prototyp. J. 28 (2022) 895–906. https://doi.org/10.1108/RPJ-08-2021-0214.

[31] G. Ginoux, I. Vroman, S. Alix, Influence of fused filament fabrication parameters on tensile properties of polylactide/layered silicate nanocomposite using response surface methodology, J. Appl. Polym. Sci. 138 (2021) 1–14. https://doi.org/10.1002/app.50174.

[32] B. Arifvianto, T.N. Iman, B.T. Prayoga, R. Dharmastiti, U.A. Salim, M. Mahardika, Suyitno, Tensile properties of the FFF-processed thermoplastic polyurethane (TPU) elastomer, Int. J. Adv. Manuf. Technol. 117 (2021) 1709–1719. https://doi.org/10.1007/s00170-021-07712-0.

[33] S.F. Costa, F.M. Duarte, J.A. Covas, Estimation of filament temperature and adhesion development in fused deposition techniques, J. Mater. Process. Technol. 245 (2017) 167–179. https://doi.org/10.1016/j.jmatprotec.2017.02.026.

[34] P. Striemann, D. Hülsbusch, M. Niedermeier, F. Walther, Optimization and quality evaluation of the interlayer bonding performance of additively manufactured polymer structures, Polymers (Basel). 12 (2020). https://doi.org/10.3390/POLYM12051166.

[35] O.Y. Gumus, R. Ilhan, B.E. Canli, Effect of Printing Temperature on Mechanical and Viscoelastic Properties of Ultra-flexible Thermoplastic Polyurethane in Material Extrusion Additive Manufacturing, J. Mater. Eng. Perform. 31 (2022) 3679–3687. https://doi.org/10.1007/s11665-021-06510-9.

[36] M. Spoerk, J. Gonzalez-Gutierrez, J. Sapkota, S. Schuschnigg, C. Holzer, Effect of the printing bed temperature on the adhesion of parts produced by fused filament fabrication, Plast. Rubber Compos. 47 (2018) 17–24. https://doi.org/10.1080/14658011.2017.1399531.

[37] J.D. Kechagias, N. Vidakis, M. Petousis, Parameter effects and process modeling of FFF-TPU mechanical response, Mater. Manuf. Process. 38 (2021) 341–351. https://doi.org/10.1080/10426914.2021.2001523.

[38] N. Garg, V. Rastogi, P. Kumar, Process parameter optimization on the dimensional accuracy of additive manufacture Thermoplastic Polyurethane (TPU) using RSM, Mater. Today Proc. 62

(2022) 94–99. https://doi.org/10.1016/j.matpr.2022.02.309.

[39] X. Gao, S. Qi, X. Kuang, Y. Su, J. Li, D. Wang, Fused filament fabrication of polymer materials: A review of interlayer bond, Addit. Manuf. 37 (2021) 101658. https://doi.org/10.1016/j.addma.2020.101658.

[40] C.Y. Liaw, J.W. Tolbert, L.W. Chow, M. Guvendiren, Interlayer bonding strength of 3D printed PEEK specimens, Soft Matter 17 (2021) 4775–4789. https://doi.org/10.1039/d1sm00417d.

[41] V. Cabreira, R.M.C. Santana, Effect of infill pattern in fused filament fabrication (FFF) 3D printing on materials performance, Rev. Mater. 25 (2020) 1–9. https://doi.org/10.1590/s1517-707620200003.1126.

[42] B. Adrover, M. Jordi, L. Ramón, J. Mesa, J.A. Travieso, Mechanical characterization of thermoplastic elastomers based on olefin processed through material extrusion, Int. J. Adv. Manuf. Technol. (2023) 323–333. https://doi.org/10.1007/s00170-023-11523-w.

[43] J. Kim, G. Kim, Effect of Rubber Content on Abrasion Resistance and Tensile Properties of Thermoplastic Polyurethane (TPU)/ Rubber Blends, 22 (2014) 523–527. https://doi.org/10.1007/s13233-014-2077-y.

[44] K. Chynybekova, S.M. Choi, Flexible patterns for Soft 3D printed fabrications, Symmetry (Basel). 11 (2019) 1–15. https://doi.org/10.3390/sym11111398.

[45] C. Chadha, G. Olaivar, M.A. Mahrous, I. Jasiuk, A.E. Patterson, Size Effects in Polycarbonate and TPU 3D-Printed via Fused Filament Fabrication, (2024). https://doi.org/10.20944/preprints202404.1649.v1.

[46] O. Bouzaglou, O. Golan, N. Lachman, Process Design and Parameters Interaction in Material Extrusion 3D Printing: A Review, Polymers (Basel). 15 (2023). https://doi.org/10.3390/polym15102280.

[47] Y. Tao, F. Kong, Z. Li, J. Zhang, X. Zhao, A review on voids of 3D printed parts by fused filament fabrication, J. Mater. Res. Technol. 15 (2021) 4860–4879. https://doi.org/10.1016/j.jmrt.2021.10.108.

Comparative Mechanical and Electrochemical Behaviour of Dissimilar Friction Stir Welded AA6082 and AA2014 Weldments

K T Thilagham[1*], D Noorullah[2]

[1]Assistant Professor, Department of Metallurgy, Government College of Engineering, Salem, 636 011, Tamilnadu, India.
*thilagham.met@gmail.com,
[2]Associate Professor, Department of Metallurgy, Government College of Engineering, Salem, 636 011, Tamilnadu, India.[2]noorullah@gcesalem.edu.in

Abstract: This paper is an experiment on the potentio-dynamic polarization behaviour of AA2014-T4 and AA6082-T651 dissimilar friction stir welds. Polarization techniques are more rapid experimental approaches as compared to conventional weight loss estimation methods for corrosion rate measurements. These activation-controlled anodic and cathodic procedures are controlled by the Tafel relationship. This linear polarization curves in the E_{corr} vs. log I_{corr} plots of AA2014-AA6082 welds were investigated for an electrochemical analyzer in 3.5% NaCl solution. Further, the AA2014 and AA6082 base metals were subjected to retrogression and reaging at 280ºC for 5 min followed by aging at 110ºC for 10 hours, then cooled under control to 10–26°C (50–500°F) before cooling with air. Then, the plates were AA2014-AA6082 friction stir welded and measured for corrosion rates. The microhardness survey had been measured for the before and after heat treated across the AA2014-AA6082 weld cross sections. The micrographs were also investigated. The microhardness and microstructure of FSW (Friction stir welded) samples were compared to the corrosion results. Henceforth, AA2014-6082 weld metal regions showed increased corrosion rate than AA2014BM and decreased corrosion rate than AA6082BM. Before heat treatment samples showed increased corrosion rates compared to after heat treatment due to the fine precipitates in the weld region.
Keywords: Dissimilar Al alloy, AA2014/AA6082, corrosion rate, Tafel plot

1. Introduction

The heat-treatable wrought alloys of the AA6082 (Al-Mg-Si) are well suited for different structural, construction, marine, mechanical, and process-equipment applications due to their moderately outstanding strength and higher corrosion resistance. As compared to alloys from other series, which include significantly smaller levels of copper, alloy AA 2014, which has copper as the primary alloying element, has poorer corrosion resistance [1-2]. The primary joining process for these alloys is FSW. FSW welding eliminates the need for further surface treatment or shielding gas. This is a well-known process with no waste, porosity, or fumes, but end-hole restrictions [3]. Previous research was helpful in determining welding settings for the dissimilar AA2014-AA6082 weld [4, 5].

The mechanical, microstructure characteristics, and corrosion behaviour of gas metal arc AA6061-T6 aluminium alloy welded joints with the impact of mechanical vibration during welding have been studied by *Ilman, M. N. et al.* Many tests, particularly electrochemical polarization tests in a solution of 3.5 percent NaCl, were conducted. A decline in intermetallic compounds like Mg_2Si in interdendritic areas, which lower local galvanic cells, may be associated with the enhanced corrosion resistance of the vibration-assisted weld joints. Base metal and HAZ may exhibit similar corrosion behaviour. The weld metal microstructure may be associated with the corrosion behaviours observed in this investigation. It can be shown that all HAZ zones in this investigation had lower corrosion current

densities than the weld metal areas. This result seems to demonstrate that the presence of Mg_2Si controls corrosion behavior [6].

Trdan, U. et al. (2012) utilized LSP (laser shock peening) on AA6082 aluminium alloy at different power densities to examine corrosion performance in a 0.6M NaCl solution. In comparison to the unprocessed samples, the results of cyclic polarization demonstrated improved passivity with corrosion current reductions of up to a factor of 12. In addition, polarization resistance after LSP was approximately seven times greater according to EIS after 24 h compared to the control sample (45 and 6.7 kΩ cm^2). Al_2O_3 enrichment, as shown by XPS analysis, helped to increase corrosion resistance while minimizing the anodic dissolution of the LSP-treated surface caused by shock waves and plasma ablation [7].

Due to two considerations, the electrochemical impact on corrosion in these alloys may be higher than in alloys of several other types: a higher change in electrode potential when there are fluctuations in the proportion of copper in the solid solution and, in certain cases, when there are non-uniformities in the concentration of the solid solution. However, these solid solution or second-phase solution-potential correlations are not principally responsible for the overall resistance to corrosion declining with increasing copper concentration. Electrochemical impact on corrosion resistance may be minimized by the development of aged or the precipitation heat treatment procedure. The quenching rate, as well as the temperature and length of artificial ageing, may all have an impact on a product's ability to resist corrosion [8].

Lumsden, J.B., et al. (1999) investigated the FSW AA7075 weld's sensitivity to corrosion. When compared to the parent metal, the microstructures showed less pitting potential and preferential grain boundary attack. The microstructure of the weld zones was characterized, and localized chemical variations within the weld zones indicated that the loss of Cu inside the precipitate-free zones and grain boundaries was associated with a drop in corrosion resistance. These findings demonstrated that a differential in pitting potentials was to account for the reduced intergranular corrosion resistance of AA 7075-T651 after FSW [9].

Buchheit,R.G., & Paglia,C.S. (2008). The microstructure becomes sensitized, exhibiting corrosion susceptibility in aluminium alloy friction stir welds. The nugget's microstructure reacts strongly to welding, and coarsening of the grain boundary precipitates encourages intergranular corrosion, which is mostly seen along the heat-affected zone of the nugget. Short-term post-weld heat treatments that decrease corrosion change the microstructure at temperatures close to those used during welding. By changing the microchemistry when welding, it is also possible to boost corrosion resistance [10].

Surekha K. et al. (2009) used salt spray and immersion tests to test the hypothesis that rotation speed has a significant impact on the rate of corrosion and the breakdown and dissolution of the intermetallic particles [12-13]. For low rotation speed welds, Jariyaboon, Manthana, et al. (2006) studied localised intergranular attack in the nugget region; for higher rotation speed welds, attack mostly happened in the heat-affected zone. Additionally, the nugget's increased cathodic reactivity as a result of the S-phase precipitation was examined [14]. Jariyaboon, Manthana, et al. (2007) studied the net anodized attack in the 7010 alloys, which had the maximum susceptibility in the nugget region. In the same way, the precipitation of the S-phase particles in 2024 provided protection to the nugget region due to its high net cathodic reactivity [15].

Ghosh, K. S. et. al. (2013) investigated the corrosion behaviour of the alloy in different electrolytes at different tempers using microstructural characteristics [11], researchers Songyi Chen et al. (2012) found that when compared to T6 temper, retrogression and reaging (RRA) increased exfoliation corrosion resistance without compromising strength [19]. İpekoğlu, G. examined how the dissimilar joints' microstructure and mechanical characteristics were affected by the initial temperature condition and PWHT [20]. According to research by Ghosh, R. et al. (2018), the fatigue performance of a material

is greatly impacted by the choice of suitable heat treatment conditions that provide control over corrosion behavior [16]. According to research by Talianker, M., and Cina, B. (1989), the reason for the SCC of 7000–T6 alloys is the removal of dislocations as a result of RR treatment [14].

According to Bin Zhou et al. (2019), the microstructure differences between T1 and T6 have a direct impact on the corrosion resistance differences. It was mentioned that the corrosion resistance of alloy samples dropped, the maximum corrosion depth increased, and the corrosion current density of T1 and T6 samples increased with an increase in chloride ion concentration [17]. Ting He et al. (2021) reported that Mg_2Si phases were anodic to their matrix and dissolved preferentially without impacting corrosion propagation considerably. The local corrosion of 6061 aluminium alloy was more affected by the AlFeSi phases than by the Mg2Si phases. The accelerated effect was stopped as the AlFeSi dissolved, and the corroded zone diameter increased to five times that of the AlFeSi phase [18]. According to Jinqiang Shan et al. (2018), each type of aluminium alloy has unique compositional proportions, meaning that various materials have different potentials. Therefore, the compositional amounts of Si and α-Al in 6082 are different. This implies that there should be less of a potential difference between Si and α-Al [19].

The above literature focused more on the corrosion studies on various zones and effects of heat treatment and precipitate particles and types of pitting, intergranular, or SCC resistance in 3.5% NaCl. These AA6082-T651 and AA2014 aluminium alloys come under heat treatable grade, where it can be given T6 temper to T74 temper were made using RRA ("Retrogression and Reaging") and DRRA ("Dual-Retrogression and Reaging"). The effects of corrosion after RRA treatment were studied by İpekoğlu, G. et.al. (2014)[20], Pengxuan Dong, et. al. (2012) [21], and Cina, B. et. al. (1989) [22]. Here, the A6082 in T651 (solution heat treatment followed by stretching and artificial ageing) and the alloys AA2014 in T4 Heat treated condition were prepared 100x50x6mm^3 test coupons for dissimilar friction stir welding. The cylindrical H13 pin is preferred. Then AA6082 plates were subjected to retrogression and reaging at 280ºC for 5 minutes, followed by aging at 110ºC for 10 hours, then cooled under control to 10–26°C (50–500°F) before cooling with air. Similar to that, the AA2014 alloy was also subjected to retrogression and reaging at 280ºC for 5 minutes, followed by aging at 110ºC for 10 hours. The plates were cooled under control to 10–26°C (50–500°F) before cooling with air.

The non-heat treated and after heat treated samples were FSW welded using welding parameters given in. Additional characterization investigations microstructure and hardness survey were conducted on the FSW samples. The objective is to study the potentiodynamic polarization behaviour of AA2014-6082 dissimilar joints in a 3.5% NaCl solution. The microstructural and microhardness were correlated with the before and after heat treated corrosion rates measured.

2.0 Experimental details

2.0Material and sample preparation

To get the chemical analysis results, aluminium AA2014 and AA6082 materials were sliced to 25x25mm^2 (1inch x 1inch) size. According to the standards, the chemical composition of AA2014 and AA6082 was verified using Vacuum Emission Spectroscopy. The chemical compositions are shown in Table 1.

Table 4.Chemical Composition (Wt%)

	Si%	Fe%	Cu%	Mn%	Mg%	Zn%	Ti%	Al%
AA6082BM	1.162	0.285	4.155	0.58	0.52	0.018	0.104	Bal.
AA2014BM	0.76	0.236	4.48	0.65	0.67	0.66	0.103	Bal.

2.1Welding parameters

In this work, the base materials were cut into work specimens of only 100x50x6mm^3 in sizes to make AA2014-AA6082 weld. The final weld dimensions of 100x100x6mm^3 were made using the welding parameters listed in Table 2. The configuration geometry of the FSW process and the tool used for the AA2014 and AA6082 welds are illustrated in Figure 1. The pin material of high speed steel with a threaded profile was used to create friction [23-24]. To improve the corrosion behaviour of the weld and metal flow [29], AA6082 was kept on the advancing side and AA2014 on the retreating side. The optimum welding parameters shown in Table 5 were used to get the AA2014 and AA6082 plates together. The RV Friction stir machines – 30 tons - axial pressure 20 kN, Coimbatore, India was used for welding [25].

Table 5.Welding parameters used for dissimilar FSW Aluminum Plates

SAMPLE NO	TOOL ROTATION SPEED (rpm)	WELDING SPEED (mm/min)
1	900	40
2	1100	60
3	1300	70
4	1500	90

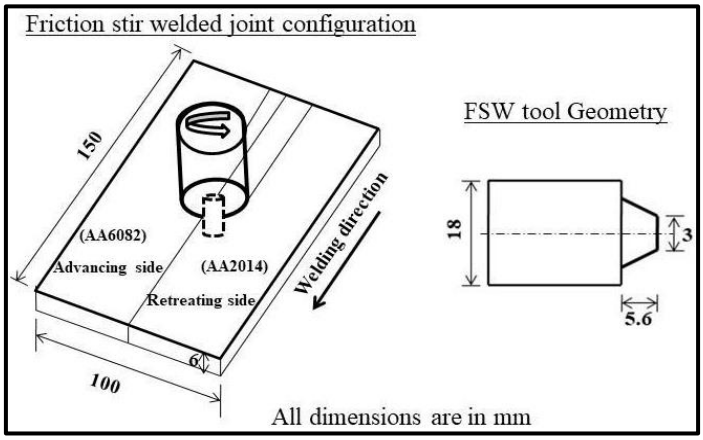

Figure 6.Configuration geometry of FSW of AA2014 and AA6082 weld

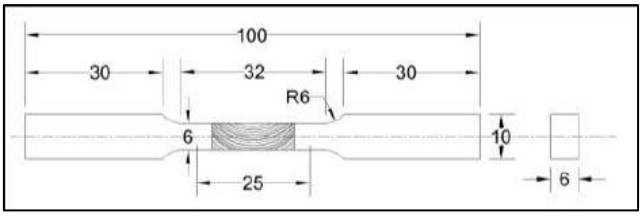

Figure 7. Standard tensile test specimen

2.2Mechanical and Microstructure studies

Figure 7 illustrates flat tensile test specimens for mechanical strength evaluation according to ASTM E8M requirements. Next, the Universal Testing machine-40T-Hydraulic machine was used to conduct the testing. The tests were conducted at room temperature (26°C) and normal atmospheric pressure, in accordance with AWS B4.0. Freshly prepared Keller's reagent (190 ml water, 5 ml HCL, 3 ml HF, 2 ml HNO_3) was utilized to etch the emery polished and mirror-finished weld to reveal the microstructures. The 100X magnified microstructures were fetched using the METZER microscope. The

microhardness was carried out with a Zwick Micro hardness tester, using 0.3 Kg weight and 15 sec dwell time given for aluminium alloys.

2.3Corrosion study

As per ASTM G 110 [26-27] to test the sample in the simulated coastal environment, the following corrosion media were prepared: 57 grams of sodium chloride, 10ml of hydrogen peroxide (30% add just prior to initiation of exposure) diluted to 1.0 liter with reagent water. To carry out the corrosion testing as per ASTM standard G 69-99 [26], 3.5 % NaCl + 30% H_2O_2 at room temperature corrosion media has been prepared.

In the Polarisation investigation was done using the GILLAC-ACM potentiostat instrument. In the experiment, a welded specimen was chosen as the working electrode, while "graphite" served as the counter electrode and Ag/AgCl as the reference electrode. In order to simulate marine conditions, an electrolyte solution comprising 3.5 percent NaCl + 30% H_2O_2 at room temperature with a potential scan rate of 0.002 V/s was used. The exposed area of the scan was 0.705 cm^2.

The anodic and cathodic Tafel slops were extended back to the plot's junction point to get I_{corr} and "Corrosion Potential" (E_{corr}). In terms of Tafel's behavior, typical cathodic polarization curves are also shown in Figure 3. The corrosion rate (mpy) was calculated using equation (1):

$$\text{Corrosion Rate (mpy)} = 3.27*10^{-3} * \frac{i_{corr} E.W.}{d} \quad \text{..... Equation (1)}$$

E.W = equivalent weight of corroding species, g

i_{corr} = corrosion current density, $\mu A/cm^2$

d = corrosion species density, g/cc

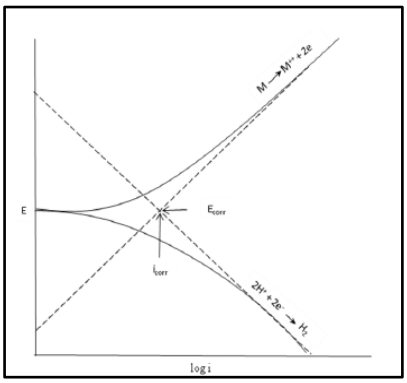

Figure 8.Tafel Plot

3.0 Results & Discussion

3.1 *Corrosion Results*

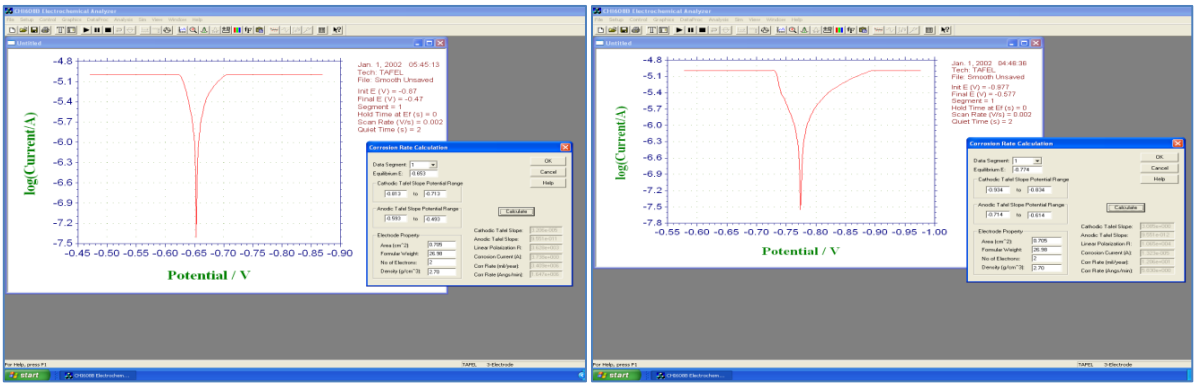

Figure 9.Corrosion results for (a) before heat treatment AA2014 base metal, (b) after heat treatment AA2014 base metal.

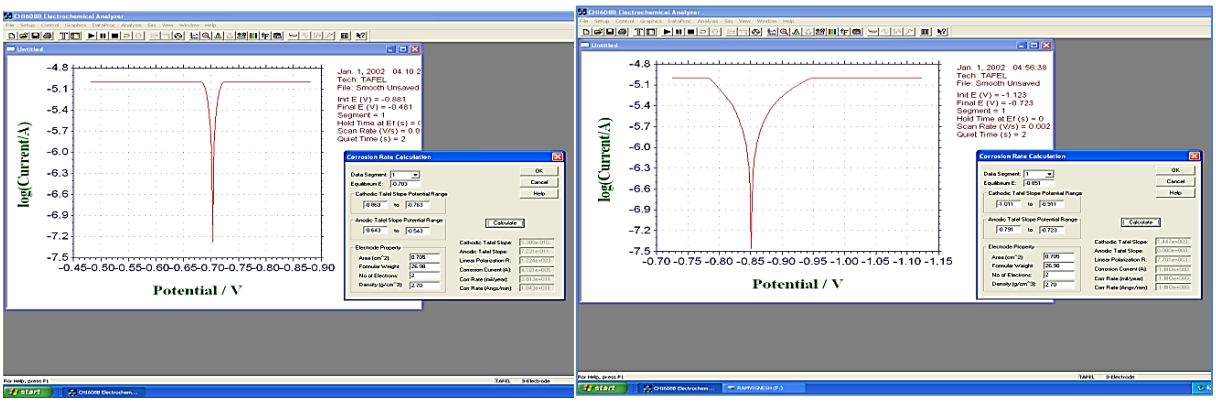

Figure 10.Corrosion results (a) before heat treatment of AA6082 base metal, (b) after heat treatment of AA6082 base metal.

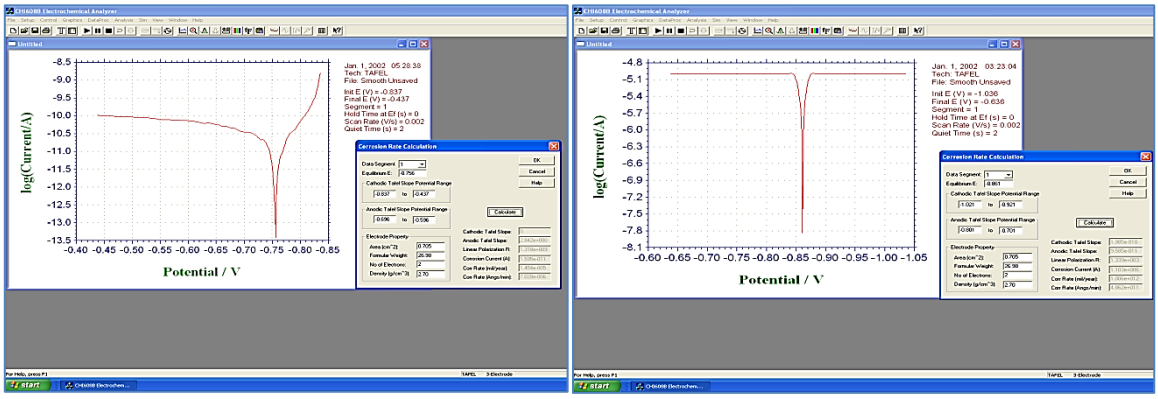

Figure 11.Corrosion results (a) before heat treatment of sample 1 weld region, (b) after heat treatment of sample 1 weld region.

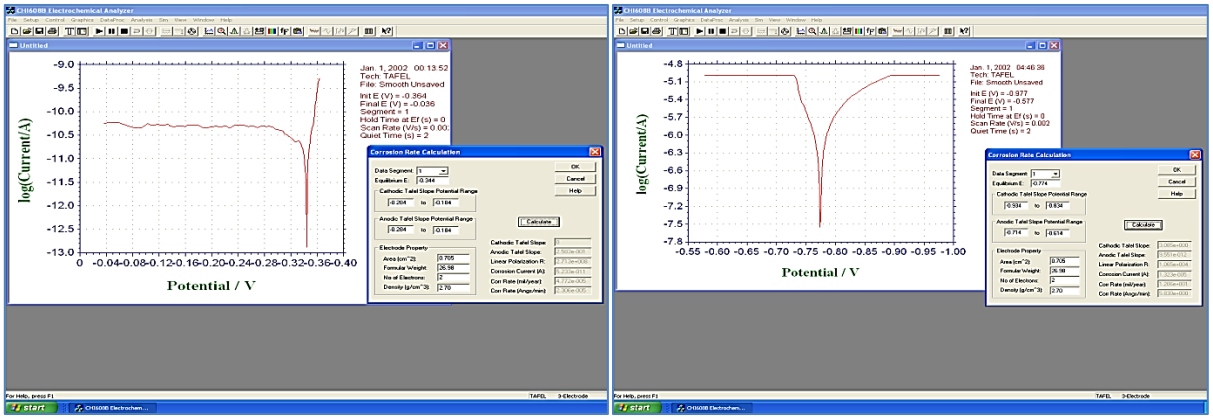

Figure 12.Corrosion results (a) before heat treatment of sample 2 weld region, (b) after heat treatment of sample 2 weld region.

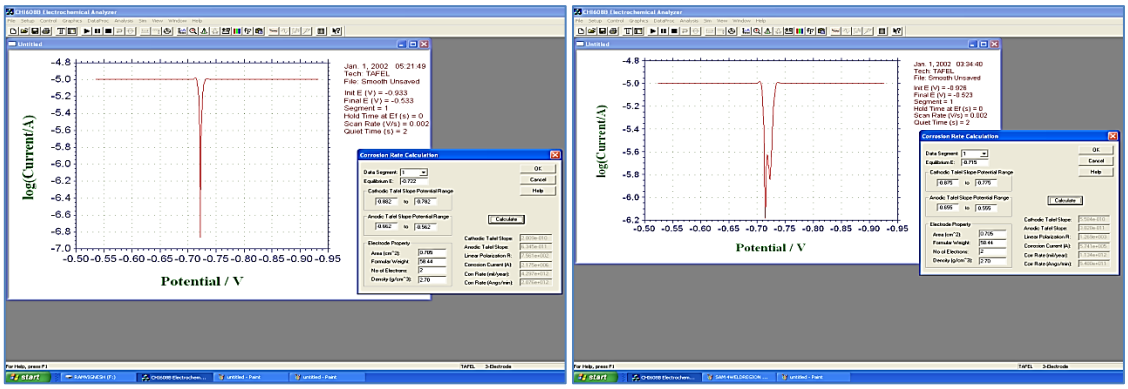

Figure 13.Corrosion results (a) before heat treatment of sample 3 weld region, (b) after heat treatment of sample 3 weld region.

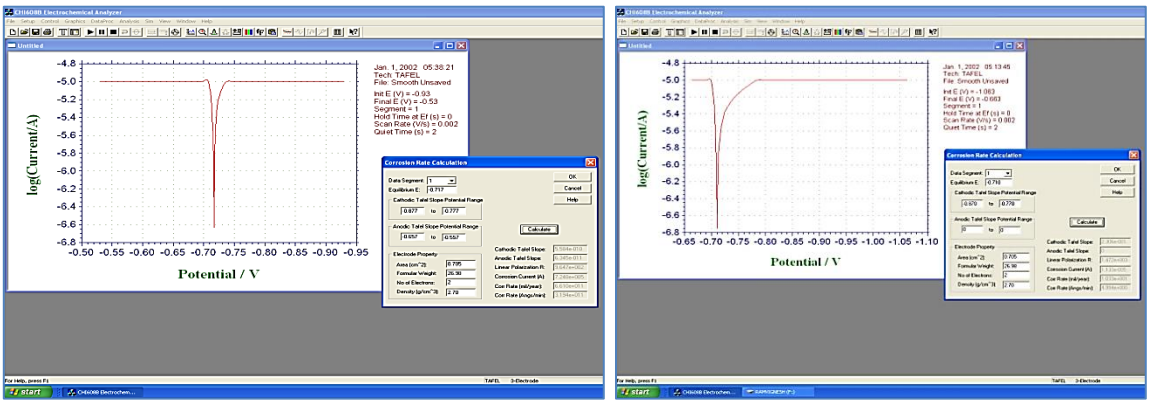

Figure 14.Corrosion results (a) before heat treatment of sample 4 weld region, (b) after heat treatment of sample 4 weld region.

Table 6. Results of E_{corr} values

Region	E_{corr} (V) Before Heat treatment	E_{corr} (V) After Heat treatment
6082BM	-0.65	-0.77
2014BM	-0.7	-0.85
Sample 1	-0.76	-0.86
Sample 2	-0.34	-0.77
Sample 3	-0.72	-0.72
Sample 4	-0.72	-0.71

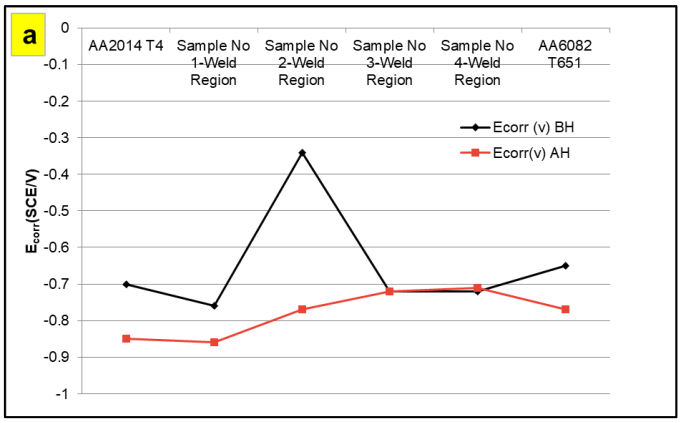

Figure 15.E_{corr} (v) values

The base metals' typical precipitate sequences are as follows:

6082 alloy is SSSS → G.P. zone → β″ → β′ → β

and 2014 alloy is SSSS → G.P. zone → θ′ → θ,

Jariyaboon, Manthana, et al. (2006) investigated the "corrosion behaviour of a friction stir weld" between two dissimilar metals (AA7010-T7651 and AA2024-T351). In immersion tests and gel visualization, the 7010 alloy's nugget area exhibited the highest susceptibility, whereas the 2024 alloy's nugget region had significant net cathodic reactivity as a result of the precipitation of S-phase particles [14]. Similarly, Shan, Jinqiang et al. (2018) shown that the Mg_2Si phase, α-Al matrix, and Si phase have corrosion potentials of -1.160, -0.876, and -0.547 SCE/V, respectively, in the sodium chloride solution. Anodically dissolving Si phase and α-Al matrix was said to occur when they set up a micro-galvanic cell. Moreover, during the formation of the microgalvanic cell, the Mg_2Si phase will dissolve first due to its lower potential than α -Al matrix [19]. Bin Zhou et al. (2019) explored a lot about how the structure of 6082 secondary particles and the Al matrix respond differently to varied electrode potentials [17].

Figure 9 shows corrosion results of before and after heat treatment of AA2014 base metal. Figure 10 shows corrosion results of before and after heat treatment of AA6082 base metal. Table 3 shows the E_{corr} (V) of the AA2014-6082 weld and base metals before and after heat treatment for 10 hours. As per Table 6, E_{corr} (V) values of AA6082 base metal showed of -0.65V for Before Heat treatment and -0.77V for after Heat treatment. Similarly E_{corr} (V) values of AA2014 base metal showed of -0.7V for Before Heat treatment and -0.85V for After Heat treatment.

Figure 14 show the Tafel curves in 3.5% NaCl solution for the AA2014-6082 weld before and after heat treatment for 10 hours. Figure 1510 shows the E_{corr} (v) values in graphical representations. So, the corrosion potential of sample 1 after heat treatment with -0.86 SCE/V and sample 2 with -0.34 SCE/V. The other regions showed intermittent values between -0.65 and -0.86 SCE/V. The least E_{corr} (v) potential values are seen mostly for after heat treatment.

Figure 15 shows the E_{corr} (v) values for both before and after heat treatment samples. It showed that after heat treatment had scanned lower corrosion potential values than before heat treatment. Figure 16 shows the E_{corr} (v) Vs. rotational speed (rpm). It showed that the increased rotational speed shows increased E_{corr} values for both before and after heat treatment samples [12]. It is also showing samples 3 and 4 with almost equal potential values for both before and after heat treatment. But sample 2 shows that before heat treatment with -0.34 V, and after heat treatment with lower potential of -0.77 V. This showed that the potential scan might be done on different phases of the AA2014-6082 weld. Similarly, the highest potential value of sample 2 before heat treatment weld regions might be also on different phase of the AA2014-6082 weld.

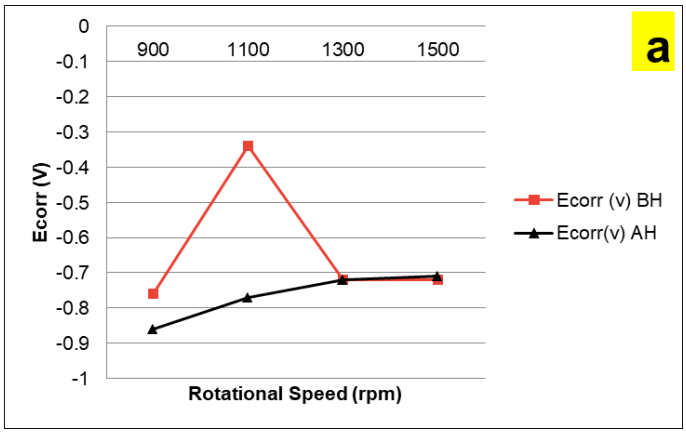

Figure 16.E_{corr} (v) Vs Rotational speed (rpm).

Table 7. i_{corr} (A/cm^2) and Corrosion Rate (mpy) values of different AA2014-AA6082 weld.

Region	E_{corr} (V)		i_{corr} (A/cm^2)		Corrosion Rate (mpy)	
	Before heat treatment	After heat treatment	Before heat treatment	After heat treatment	Before Heat treatment	After Heat treatment
AA2014 T4 BM	-0.7	-0.85	3.74E+00	1.32E-05	3.41E+06	1.21E+01
Sample No 1-Weld Region	-0.76	-0.86	1.60E-11	1.10E+05	1.45E-05	1.01E+12
Sample No 2-Weld Region	-0.34	-0.77	5.23E-11	1.35E-05	4.77E-05	1.21E+01
Sample No 3-Weld Region	-0.72	-0.72	2.18E+06	5.74E+05	4.30E+12	1.12E+12
Sample No 4-Weld Region	-0.72	-0.71	7.25E+05	1.13E+05	6.61E+11	1.03E+01
AA6082 T651 BM	-0.65	-0.77	4.95E+06	8.03E+00	3.25E+11	1.48E+00

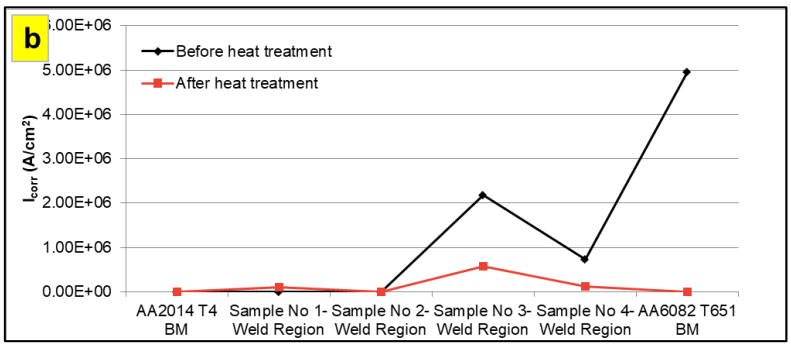

Figure 17. Potentio-dynamic polarization i_{corr} (A/cm^2) comparison of various regions of weld cross section before and after heat treatment.

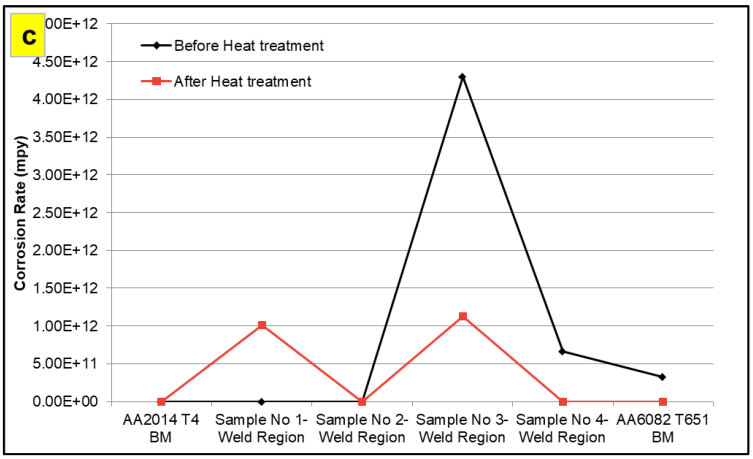

Figure 18. Corrosion Rate (mpy) comparison of various regions of weld cross section before and after heat treatment

Table 7 shows the i_{corr} (A/cm^2) and Corrosion Rate (mpy) values of different AA2014-AA6082 welds. Figure 9 show the Potentio-dynamic polarization i_{corr} (A/cm^2) and corrosion Rate (mpy) comparisons of various regions of the weld in a 3.5% NaCl solution. From, it was observed that the decreased corrosion rates for after heat treatment [29].

Figure 18 shows the increased corrosion density of 2.18E+06 A/cm^2 for sample 3 before heat treatment weld. Lowest current density of 1.60E-11 A/cm^2 was observed for sample 1. It was observed that the corresponding corrosion rate also increased. Lower current density 1.45E-05 mpy of sample 1 was showing lowest corrosion rate. Before heat treatment Sample 3 had showed corrosion rate of 4.30E+12 mpy. Similarly, increased corrosion density of 5.74E+05 A/cm^2 was observed for sample 3 after heat treatment. It showed the corrosion rate of 1.12E+12 mpy. The lower current density of 1.35E-05 A/cm^2 was observed for sample 2 after heat treatment and the corresponding corrosion rate was 1.21E+01 mpy.

The weld metal regions were showed increased corrosion rates, when compared to the AA2014 base metal and but decreased with respect to AA6082 base metal regions, due to fine precipitates formation in the weld.

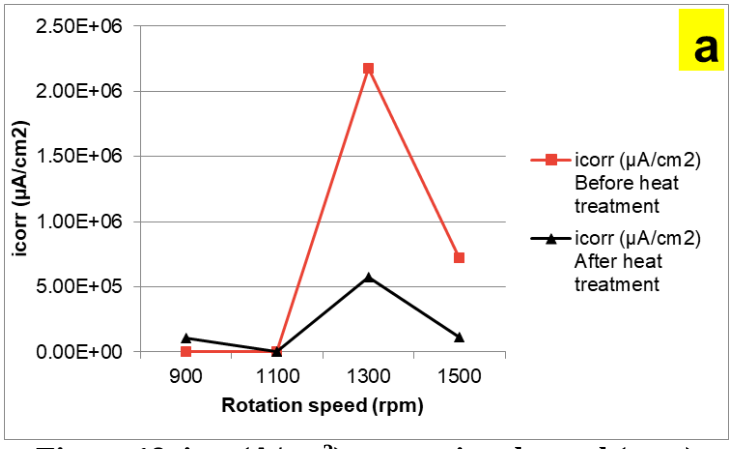

Figure 19. i_{corr} (A/cm^2) vs rotational speed (rpm)

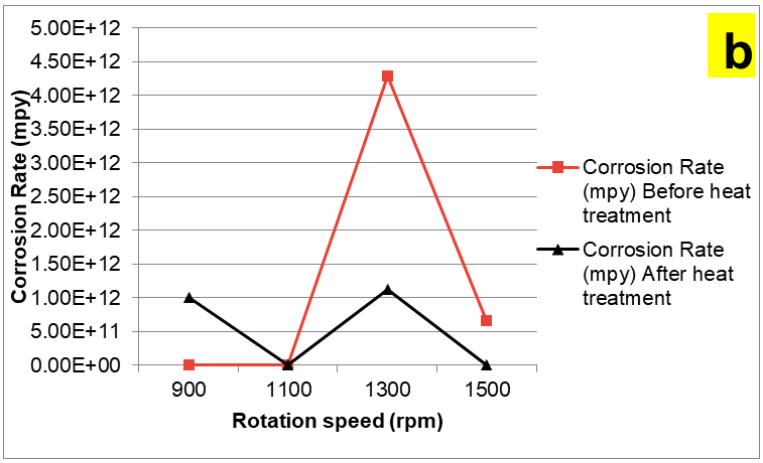

Figure 20. Corrosion rate(mpy) vs rotational speed (rpm)

Figure **18**14-15 show that i_{corr} (A/cm^2) vs rotational speed (rpm) and corrosion rate (mpy) vs rotational speed (rpm) respectively. According to K. Surekha et al. (2009) found that improved resistance was indicated by the i_{corr} values decreasing as rotation speed increased [12-13]. The I_{corr} represents the kinetic process of the electrode reaction, whereas the E_{corr} represents the thermodynamic process. I_{corr} is a crucial measurement in determining a material's corrosion resistance. It was noted that the smaller the I_{corr}, the greater the material's corrosion resistance [31]. The lowest corrosion potential and increasing current density indicate the worst corrosion resistance [32]. Thus, the worst corrosion rate was seen for sample 3 before heat treatment AA2014-6082 weld region.

The i_{corr} and corrosion rate showed that after heat treatment with improved corrosion resistance. Thus, the corresponding corrosion rate of the sample after heat treatment also showed increased corrosion resistance. It showed that the i_{corr} values were non-linear with the applied rotational speed. It might be due to the cathodic reactivity of 2014BM matrix, the anodic activity of 6082 base metal matrix and/or its intermetallic phase–matrix microgalvanic cells across the scanned area.

3.2 *Mechanical and Microstructure Analysis*

Table 8.Tensile strength values of the samples.

		Before Heat treatment (HV)	Fracture Location		After heat treatment (HV)	Fracture Location
Sample no 1 - weld region		189	Fracture at HAZ near AA6082		143	Fracture at HAZ near AA6082
Sample no 2 - weld region		171	Fracture at weld zone		86.5	Fracture at weld zone

Sample no 3 - weld region		180	Fracture at weld zone		136	Fracture at weld zone
Sample no 4 - weld region		207	Fracture at HAZ near AA6082		150.4	Fracture at HAZ near AA6082

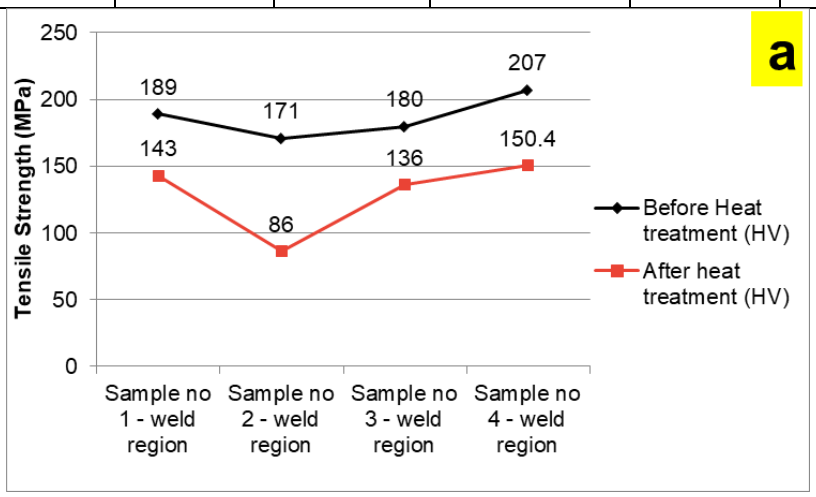

Figure 21.Graphical representation of Tensile strength values

Table 8 and Figure 21 show the tensile strengths before and after heat treated samples. Sample 3 showed the highest strength of 207 MPa for the before heat treatment and 150.4 MPa for the after Heat treatment. Sample 1 showed that the lowest strength of 171 MPa for the before heat treatment and 86.5 MPa for the after heat treated sample. The increased strength was seen for before heat treatment samples.

Figure 22 (a), (b) show the before and after heat treatment microstructures of AA6082 base metal. It shows the α-Al matrix with its Al-Mg-Si intermetallics. Figure 23 (a), (b) show the before and after heat treatment microstructures of AA2014 base metal. It showed that the α-Al matrix with its Al-Cu intermetallics.

Figure 24 (a), (b) show the before and after heat treatment microstructures of sample 1 weld region. Figure 24 (c), (d) show the before and after heat treatment microstructures of sample 2 weld region. Figure 25 (a), (b) show the before and after heat treatment microstructures of sample 3 weld regions. Figure 25 (c), (d) show the before and after heat treatment microstructures of sample 4 weld regions. In weld, it was observed with more AA6082 precipitates. So, it was evidently seen that both the base metal and weld regions with more dark precipitates in after heat treatment regions. This precipitate formation was reason for increased corrosion resistance for after heat treatment.

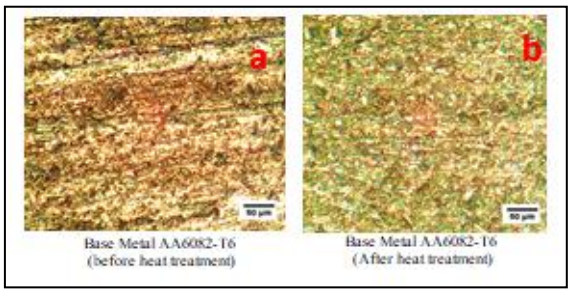

Figure 22.Microstructures of AA6082 base metal before and after heat treatment.

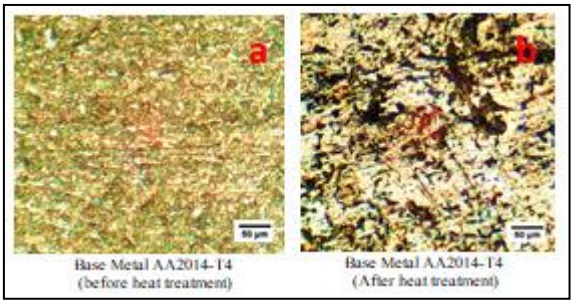

Figure 23.Microstructures of AA2014 base metal before and after heat treatment.

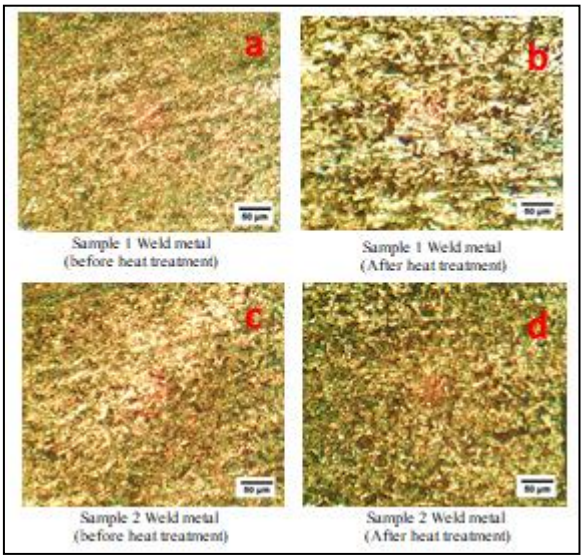

Figure 24.Microstructure of weld metals Sample 1 and Sample 2 AA2014 and AA6082 weld before and after heat treatment

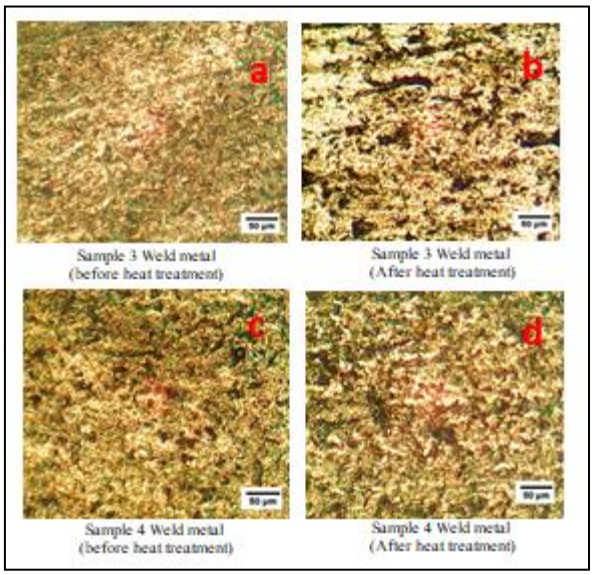

Figure 25.Microstructure of weld metals Sample 3 and Sample 4 AA2014 and AA6082 weld before and after Heat treatment

3.3 *Hardness Survey*

Table 9. Hardness survey of Sample 1

Sample	Distance from the weld center (mm)	15	10	5	0	-5	-10	-15
Sample 1	Before heat treatment (HV)	46.2	47.3	118.6	99.7	88.7	80.8	78.7
	After heat treatment (HV)	37.5	40.3	57.5	60.2	57.5	57.5	57.5
Sample 2	Before heat treatment (HV)	38.1	42.4	105.3	67.3	77.4	73.7	70.8
	After heat treatment (HV)	38.1	36.8	50.5	43.6	67.5	80.8	82.5
Sample 3	Before heat treatment (HV)	46.4	48.1	90.1	81.2	93.5	90.8	72.8
	After heat treatment (HV)	37.5	40.3	48.4	69	68.4	75.8	80.5
Sample 4	Before heat treatment (HV)	38	43.2	120.5	98.2	78.4	85.8	75
	After heat treatment (HV)	37.5	42.3	56.4	71.2	67.4	80.5	81.2

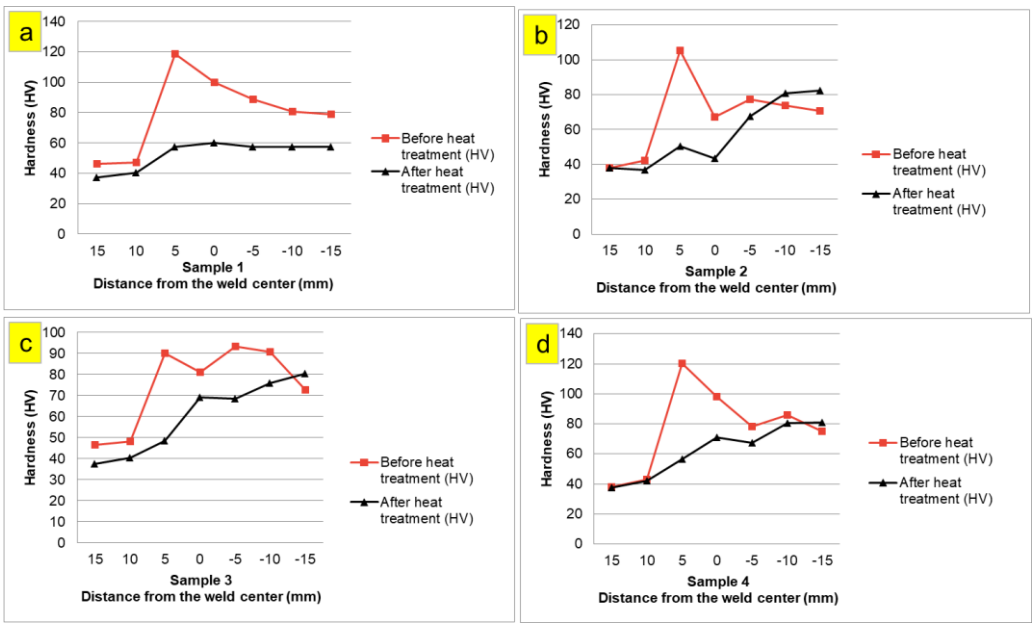

Figure 26.Hardness comparison for sample 1-4.

Table 96 shows the hardness survey taken across AA2014-AA6082 weld cross sections of Samples 1 to 4. Figure 26(a-d) showed that the graphical representations of the hardness survey of all the AA2014-AA6082 welds. HM Lieth, et al. (2006) carried out research on the behaviour of the microstructure, corrosion rate, and mechanical properties of API 5L X60 steel in three different environments: (i) freshwater; (ii) seawater; and (iii) crude oil. Following the austenitization at 900°C and

800°C, the quenching was carried out at 600°C, 450°C, and 300°C. It may be deduced that when tempering temperatures increased, the microhardness values decreased [28].

Here, the results revealed that the sample 4 weld region has a high hardness of 120.5HV and the lower hardness of 90.1HV, due to the trailing side heat transfer effect [29]. Also, advancing side increasing hardness was due to the dynamic recovery and recrystallization effects of friction stir welding on AA2014-6082 weld cross section.

The hardness survey across the FSW sample showed lower hardness for after heat treatment of 10 hours at 110 ºC. This was due to more precipitate out after heat treatment. Lower hardness revealed on sample 2 after heat treatment in weld is due the over aged precipitates formation on that region. Similarly, the lowest hardness of 48.4HV after heat treatment is due to the over aged precipitate formation on the sample 1 AA2014-6082 weld.

Figure 617-20 microstructures of AA2014-6082 weld and base metal regions were also showing after heat treatment with recrystallized fine precipitates. The microstructures of after heat treatment are due to more precipitates of that (AA2014-6082) alloy showing increased corrosion rates.

So, it is also concluded that more than the hardness and tensile strength, the microstructural features are associated with the corrosion potential, current density and corrosion rates.

4.0 Conclusions

The AA2014-T4 and AA6082-T651 weldments, which were welded using a dissimilar FSW process, were corrosion analyzed before heat treated and after heat treated that is retrogression and reaging at 280 ºC for 5 minutes followed by aging at 110 ºC for 10 hours, samples respectively. The results showed a decreased Potentio-dynamic polarization corrosion rate after tempering treatment. The weld metal region showed increased corrosion rates, when compared to the AA2014 base metal and but decreased with respect to AA6082 base metal regions, due to fine precipitates formation in the weld. In microstructure, the AA2014-AA6082 weld metals were observed with more AA6082 precipitates. The hardness survey results showed that the sample near the AA6082 base metal region had a high hardness and the AA2014 base metal region had a lower hardness because of the trailing side heat transfer effect. The hardness survey across the FSW sample showed decreased hardness after tempering for 10 hours at 110 ºC. This was due to more over aged precipitate formation on the advancing side.

Henceforth, AA2014-6082 weld metal regions showed increased corrosion rate than AA2014BM and decreased corrosion rate than AA6082BM. Before heat treatment samples showed increased corrosion rates compared to after heat treatment due to the fine precipitate formation in the weld region. It is also concluded that more than the hardness and tensile strength, the microstructural features are associated with the corrosion potential, current density and corrosion rates.

References

[1] Mishra, Rajiv S., and Z. Y. Ma. "Friction stir welding and processing." Materials science and engineering: R: reports 50.1-2 (2005): 1-78.

[2] Kou, S.(2003).Heat flow in welding. Welding Metallurgy, Second Edition, pp.37-64.

[3] Raheem Al-Sabur, Tensile strength prediction of aluminium alloys welded by FSW using response surface methodology – Comparative review, Materials Today: Proceedings, Volume 45, Part 6, 2021, Pages 4504-4510.

[4] ÇAVUŞ, Emre Can; KOÇAR, Oğuz. Mechanical behavior of AA5083/AA6061 friction stir welds using modal analysis. Materials Testing, 2023, 65.6: 961-971.

[5] Kocar, O., Yetmez, M., Baysal, E., & Ozyigit, H. A. (2022). Mechanical behavior of a friction

welded AA6013/AA7075 beam. Materials Testing, 64(2), 284-293.

[6] Ilman, M. N., Widodo, A., & Triwibowo, N. A. (2022). Metallurgical, mechanical and corrosion characteristics of vibration assisted gas metal arc AA6061-T6 welded joints. Journal of Advanced Joining Processes, 6, 100129.

[7] Trdan, U., & Grum, J. (2012). Evaluation of corrosion resistance of AA6082-T651 aluminium alloy after laser shock peening by means of cyclic polarisation and ElS methods. Corrosion Science, 59, 324-333.

[8] Lumsden, J. B., Mahoney, M. W., Pollock, G., & Rhodes, C. G. (1999). Intergranular corrosion following friction stir welding of aluminum alloy 7075-T651. Corrosion, 55(12).

[9] Patil, H. S., & Soman, S. N. (2014). Corrosion behaviour of friction stir welded aluminium alloys AA6082-T6. American Journal of Materials Engineering and Technology, 2(3), 29-33.

[10] Paglia, C. S., & Buchheit, R. G. (2008). A look in the corrosion of aluminum alloy friction stir welds. Scripta Materialia, 58(5), 383-387.

[11] Ghosh, K. S., Hilal, M., & Sagnik, B. O. S. E. (2013). Corrosion behavior of 2024 Al-Cu-Mg alloy of various tempers. Transactions of Nonferrous Metals Society of China, 23(11), 3215-3227.

[12] Surekha, K. &Murty, B. &Kalvala, Prasad. (2009). Effect of processing parameters on the corrosion behaviour of friction stir processed AA 2219 aluminum alloy. Solid State Sciences - SOLID STATE SCI. 11.

[13] Surekha, K. &Murty, B. & Kalvala, Prasad. (2011). Comparison of corrosion behaviour of friction stir processed and laser melted AA 2219 aluminium alloy. Materials & Design - MATER DESIGN. 32. 4502-4508.

[14] Jariyaboon, Manthana& Davenport, Alison & Ambat, Rajan & Connolly, B. & Williams, S. & Price, D.. (2006). Corrosion of a dissimilar friction stir weld joining aluminium alloys AA2024 and AA7010. Corrosion Engineering, Science and Technology. 41. 135-142.

[15] Jariyaboon, Manthana& Davenport, Alison & Ambat, Rajan & Connolly, B.J. & Williams, S.W. & Price, D.A.. (2007). The effect of welding parameters on the corrosion behaviour of friction stir welded AA2024–T351. Corrosion Science. 49. 877-909.

[16] Ghosh, R., Venugopal, A., Rao, G.S. et al. (2018). Effect of Temper Condition on the Corrosion and Fatigue Performance of AA2219 Aluminum Alloy. J. of MateriEng and Perform 27, 423–433.

[17] Zhou, B., Zhang, C., Yang, L., Bai, D., & Olugbade, E. O. (2020). Corrosion behaviour and mechanism of 6082 aluminium alloy in NaCl and Na2SO4 etchants. Materials and Corrosion, 71(3),

392-400.

[18] He T, Shi W, Xiang S, Huang C, Ballinger RG. Influence of Aging on Corrosion Behaviour of the 6061 Cast Aluminium Alloy. Materials. 2021; 14(8):1821.

[19] Shan, Jinqiang & Xin, Xiucheng & Zhang, Chi & Cao, Guohua & Yang, Li & Huang, Genzhe. (2018). Microstructural Analyses of Inter-Granular Corrosion Behavior for 6082-T6 Aluminum Alloy. IOP Conference Series: Materials Science and Engineering. 301. 012074.

[20] İpekoğlu, G., Çam, G. (2014).Effects of Initial Temper Condition and Postweld Heat Treatment on the Properties of Dissimilar Friction-Stir-Welded Joints between AA7075 and AA6061 Aluminum Alloys. Metall Mater Trans A 45, 3074–3087.

[21] Songyi Chen, Kanghua Chen, GuoshengPeng, Le Jia, Pengxuan Dong, (2012). Effect of heat treatment on strength, exfoliation corrosion and electrochemical behavior of 7085 aluminum alloy, Materials & Design, Volume 35, 2012, Pages 93-98.

[22] Talianker, M., Cina, B. (1989).Retrogression and reaging and the role of dislocations in the stress corrosion of 7000-type aluminum alloys. Metall Mater Trans A 20, 2087–2092.

[23] Thilagham, K. T., & Muthukumaran, S. (2019). Process parameter optimization and characterization studies of dissimilar friction stir welded advancing side AA6082-T6 with retreating side AA2014-T87. *Materials Today: Proceedings*, *27*.

[24] Gunasekaran, P., Thilagham, K. T., & Noorullah, D. (2020). Studies on friction stir welding of AA2014, AA6082 and AA7075 simillar and dissimillar joints. In *Advanced Engineering Forum* (Vol. 37, pp. 15-24).

[25] Thilagham, K. T., & Muthukumaran, S. (2022). Center Stir Zone Investigations of Dissimilar AA6082, AA2014 and AA7075 Welds. IntechOpen.

[26] "Standard Test Method for Determining the Susceptibility to Intergranular Corrosion 5XXX series Aluminium alloys by Mass loss after exposure to Nitric acid(NAMLT test)", G 67- 99, pp 269-270.

[27] "Standard Test method for Measurement of corrosion potentials of aluminium alloys", G 69-97, pp 272-274.

[28] "Standard Practice for Evaluating Intergranular corrosion resistance of heat treatable aluminium alloys by immersion in sodium chloride plus hydrogen peroxide solution", G 110-92, Annual book of ASTM standards, American society for testing and materials. pp 487-489.

[29] Khalaf HI, Al-Sabur R, Abdullah ME, Kubit A, Derazkola HA. Effects of Underwater Friction Stir Welding Heat Generation on Residual Stress of AA6068-T6 Aluminum Alloy.

Materials. 2022; 15(6):22-23.

[30] Lieth, H. M., Al-Sabur, R., Jassim, R. J., & Alsahlani, A. (2021). Enhancement of corrosion resistance and mechanical properties of API 5L X60 steel by heat treatments in different environments. Journal of Engineering Research, 9(4B).

[31] Yang, L., Yang, S., & Huang, G. (2021, March). Investigation of Electrochemical Corrosion Behaviour of 6082 Aluminum Alloy under Simulated Deicing Agent Conditions. In Journal of Physics: Conference Series (Vol. 1838, No. 1, p. 012004). IOP Publishing.

[32] Pang Q, Zhao M, Hu Z-L. Effect of Deformation on the Corrosion Behavior of Friction Stir Welded Joints of 2024 Aluminum Alloy. Materials. 2022; 15(6):2157.

INVESTIGATION OF MICROSTRUCTURE AND MECHANICAL PROPERTIES OF CuCo1Ni1Be ALLOY FORMED BY ROLLING AND FORGING METHOD

Feyzanur Öztürk[1], Volkan Karakurt[1], Talip Çitrak[1], Gamze Nur Gözüak[1], Feriha Birol[1], Orçun Zığındere[1],

[1]Sağlam Metal San. Ve Tic. A.Ş.

Abstract

Cu-Be alloys are high strength, high performance in corrosive environments and resistant to high temperatures. They also have high thermal and electrical conductivity properties. Thanks to these properties, CuCo1Ni1Be alloy, which is a Cu-Be alloy, is used in spot welding electrodes of stainless steel, monel and nickel alloys, as inserts in plastic injection molds, in plastic blow molds, cooling cores and other parts, as seam heads in plastic packaging, as permanent molds in casting alloys such as copper, brass, bronze and in spot electrodes of steel mesh machines. CuCo1Ni1Be material can be easily processed by both hot and cold forming methods and produced in various forms and sizes. Therefore, it is widely used in many industries. In this study, the microstructural, mechanical and wear properties of CuCo1Ni1Be alloy formed by two different methods, hot forging and hot rolling, were investigated comparatively. Hardness, electrical conductivity, tensile and wear tests were applied to the materials subjected to heat treatment after hot forming, and the results obtained were examined. As a result of the mechanical and wear tests, it was observed that the CuCo1Ni1Be alloy formed by the hot forging method exhibited a superior combination of strength and ductility, as well as better wear resistance compared to the alloy formed by rolling. The study's findings suggest that applying hot forging at low deformation rates and proper heat treatment can result in a better combination of material properties. This can lead to improved efficiency and longer service life for the materials in their intended applications.

Keywords: CuCo1Ni1Be, Forging, Rolling, Microstructure, Mechanical Test

1. Introduction

CuCo1Ni1Be alloy is a class of Cu-Be alloy with a combination of good electrical conductivity, high-temperature resistance, good corrosion resistance and high strength. These properties give CuCo1Ni1Be alloy a wide range of applications from automotive to nuclear energy [1]. The nickel element added to the alloy increases the electrical conductivity of the alloy, while the addition of cobalt improves the strength of the alloy. CuCo1Ni1Be alloy, which is a precipitation hardening alloy, can be shaped by various hot and cold plastic forming methods such as rolling, forging, extrusion, ECAP [2-3].

In the aging process of CuBe alloys, the precipitation sequence proceeds as supersaturated solid solution → Guinier-Preston (GP) zones → γ'' → γ' → γ (Cu-Be) transformation [4]. CuCo1Ni1Be alloy belongs to the group of CuBe alloys containing Co and Ni. It exhibits precipitation hardening, resulting in the precipitation of phases with various compositions of Co, Ni, and Be, which are called beryllides. . The precipitates formed by cobalt and nickel with beryllium, which are decomposed during solidification, are called primary beryllites and are easy to identify under an optical microscope. Another beryllite formed

as a result of precipitation of intermediate phases is called secondary beryllites. They cannot be observed under an optical microscope because of their nano dimensions. The strong affinity of cobalt for beryllium, compared to nickel, tends to precipitate as beryllite phase by forming a compound with beryllium instead of forming a solid solution in the matrix. In addition, depending on the amount of cobalt, ternary $CoNiBe_x$ beryllites can also be formed [5].

CuCo1Ni1Be alloy is produced by various hot and cold plastic forming methods such as rolling, forging, extrusion, ECAP. The condensation of voids and the increase in dislocation density due to plastic deformation facilitate the nucleation of precipitates during aging. This leads to increased dispersion of precipitates during aging, which significantly affects the strain hardening of alloys [6].

The most common hot-forming methods used for copper alloys are hot forging and rolling. However, hot forging is limited to short profiles. For long profiles hot rolling is an efficient process. Although both methods are hot-forming processes, parameters may need to be optimized to achieve the same material properties. The most common hot-forming methods used for copper alloys are hot forging and rolling. However, hot forging is limited to short profiles. For long profiles hot rolling is an efficient process. Although both methods are hot-forming processes, parameters may need to be optimized to achieve the same material properties. Wanneng Liao et al [7] investigated how different plastic deformation methods affect the strength and electrical conductivity of a copper-based alloy. They reported that the hardness and electrical conductivity of the material are affected depending on dislocation density, precipitation behavior and the resulting grain size with the change of plastic deformation method.. A study at Sağlam Metal is ongoing for process parameter optimization including deformation ratios to achieve long profiles with the same properties as short profiles.In this study as a part, the effect of the same deformation ratio (40%) on the properties of hot forged and hot rolled CuCo1Ni1Be alloy was presented. Microstructural examinations, hardness, electrical conductivity and wear tests were carried out and the effect of hot deformation method for the same deformation ratio was discussed by comparing the results obtained.

2. Materials and Method

CuCo1Ni1Be alloys were subjected to plastic deformation by 40% forging in the temperature range 850-900 °C. The rolling process was carried out with a laboratory scale rolling machine at Karabük University with a 40% deformation rate from 20 mm thickness to 12 mm thickness after annealing in the furnace at 875°C for 1.5-2 hours. Hot forging under the same conditions was carried out at Sağlam Metal. Afterward, the samples underwent solution heat treatment at 960°C for 45 minutes, followed by quenching in water, and then were aged at 470°C for 6 hours."The heat treatment graph of the materials is given in Figure 1.

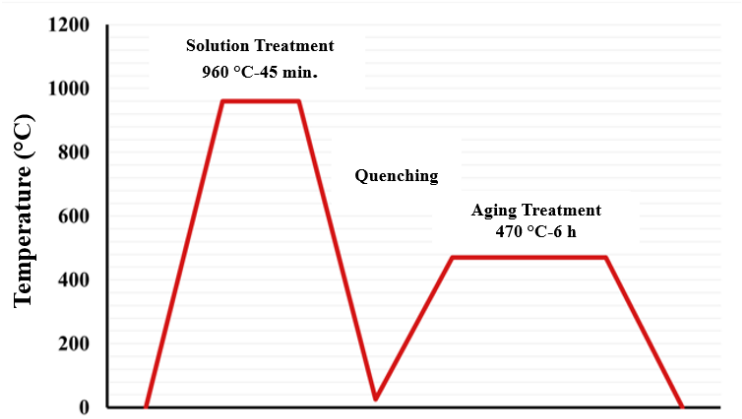

Figure 1. Heat treatment graph of CuCo1Ni1Be materials.

Microstructure characterizations were performed using a Nikon LV150N flat metal microscope. For metallographic examinations, the samples were first sanded with sandpaper in the range of 350, 600, 800, 1200, 2500 grit. Then, they were polished with 3 µm and 1 µm diamond paste. After etching, the samples were submitted to the microstructuralexamination. Grain size analyses of the forged and rolled samples were performed using Clemex Vision Lite Image Analysis Software according to ASTM E112-13 standard.

The hardness of the materials after heat treatment was measured with AFFRI-330 RSD device. Rockwell B hardness tests were performed with a diamond conical tip under 10 kg pre-load, 100 kg 1st main load and 150 kg 2nd main load.

Wear tests were carried out using the linear wear tester available at Sağlam Metal. The wear test was applied to the materials in a dry environment, at a speed of 150 Rpm and at a distance of 450 meters under a load of 20 N using a 100Cr6 ball. Before and after the test, the weight was measured on a precision balance with a precision of 0.0001, and the weight loss of the materials was determined.

3. Results and Discussion

3.1. Microstructure

Figure 2 show optical microscope images of CuCo1Ni1Be alloys formed by forging and rolling at 100X and 500X magnifications. It was observed that the rolling-formed material exhibited a finer microstructure compared to the forging-formed material . The beryllite phases precipitated into the matrix tended to precipitate more at the grain boundaries in the rolling-formed material compared to the forging-formed material.

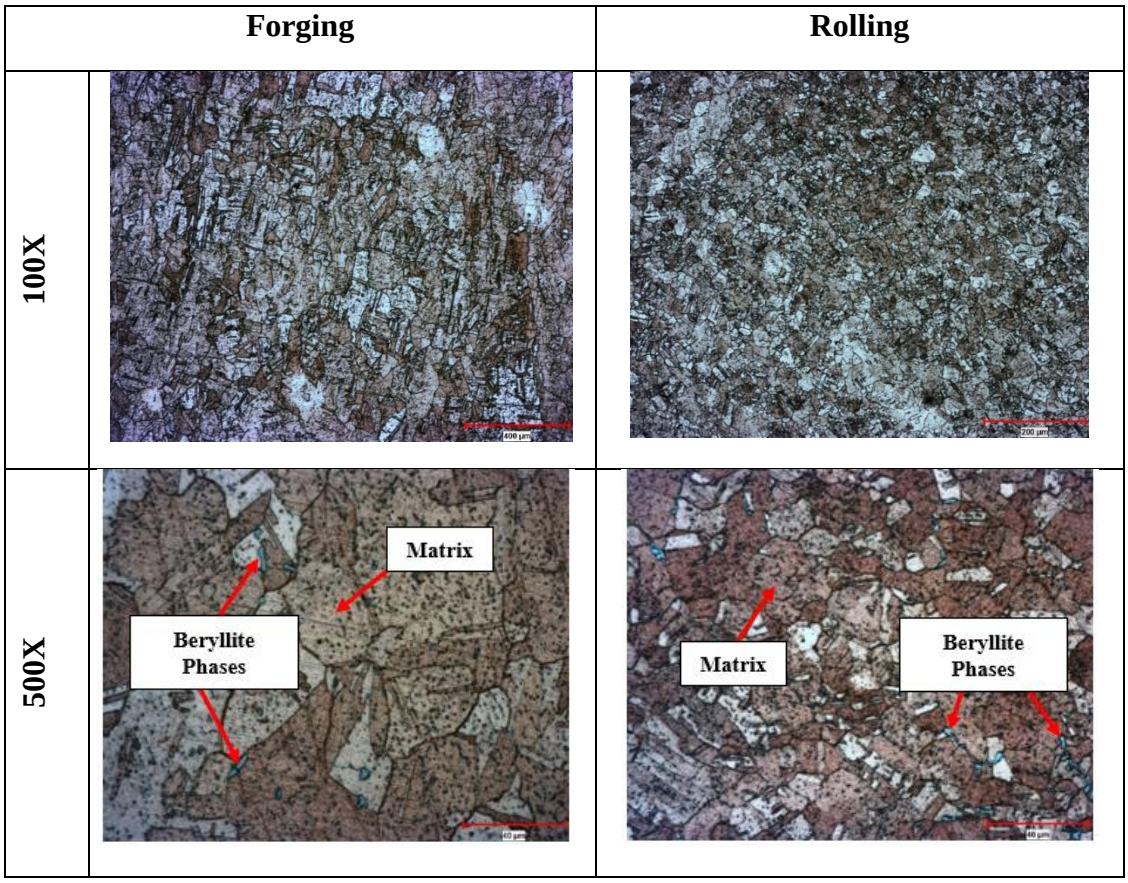

Figure 2. Optical microscope images of hot forged and hot rolled CuCo1Ni1Be alloy at 100X and 500X Magnification.

The results of the grain size analysis are given in Table 1. The average grain size of the material shaped by forging and hot Rolling was found to be 66.43 µm and 21.83 µm respectively. When the grain size analysis was performed in the rolling method, the smaller average grain size is thought to be since a more homogeneous deformation can be applied at one time with hot rolling compared to hot forging method.

Table 1. Average grain size results of CuCo1Ni1Be alloy formed by forging and rolling.

CuCo1Ni1Be	Average Grain Size (µm)
Forged	66,43
Rolled	21,83

3.2. Hardness and Electrical Conductivity Test Results

The hardness and electrical conductivity results of CuCo1Ni1Be alloys formed by rolling and forging are given in Figure 3 and 4. The hardness of the forging-formed material was measured as 101.6 HRB, while the electrical conductivity was measured as 25.3 MS/m. The hardness of the material shaped by rolling was measured as 97.8 HRB, while the electrical conductivity was measured as 27.3 HRB. The hardness of the forged material was found to be higher than that of the rolled material, while the

electrical conductivity was found to be lower. In alloys hardened by precipitation hardening, the lower the solid solubility, the higher the electrical conductivity. Secondary phase particles precipitated in the matrix also add hardness and strength to the material. However, strength and electrical conductivity are known to be inversely proportional parameters. The increase in the severity of plastic deformation causes a decrease in electrical conductivity due to distortions in the lattice structure [8-10].

The fact that the hardness of the material shaped by forging is higher than the material shaped by rolling, but the electrical conductivity is lower isconsistent with the literature. In this study, although the same deformation rate and heat treatment parameters were applied in forging and rolling methods, this difference in hardness and electrical conductivity is thought to be due to the different plastic deformation method.

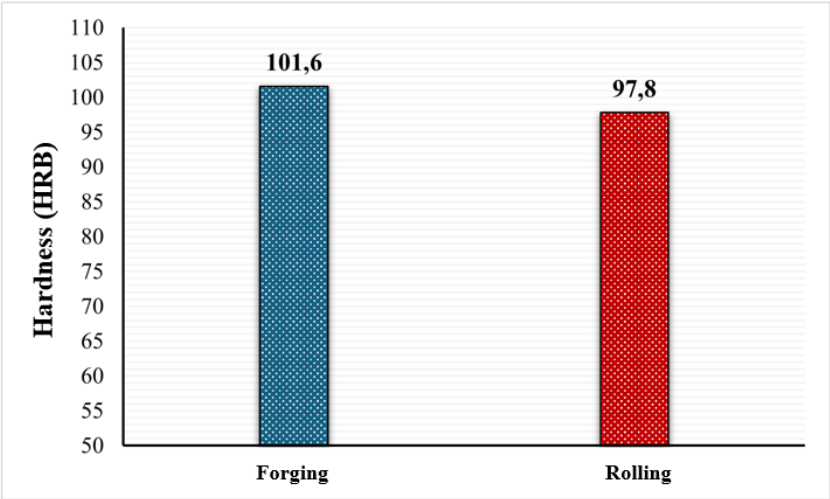

Figure 3. Hardness test results of CuCo1Ni1Be alloy formed by forging and rolling.

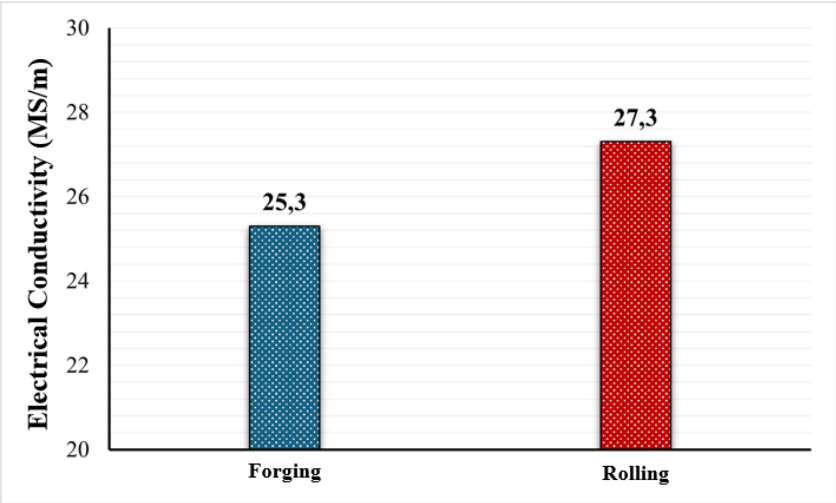

Figure 4. Electrical conductivity test results of CuCo1Ni1Be alloy formed by forging and rolling.

3.4. Wear Test Results

The weight losses of CuCo1Ni1Be alloys deformed 40% by forging and rolling are given in Figure 5 as a result of the wear test performed at 150 rpm speed, 450 meters distance, under 20N load. As a result of

the wear test, the weight lossesof the material formed by forging and hot Rolling were found to be 0.0605 g and 0.0884 g respectively. The hot forged sample revealed lower weight loss indicating higher wear resistance. The lower weight loss of the forged material may be explained its microstructure and higher hardness. The forged samples exhibited a more uniform phase distribution within the matrix compared to the hot rolled samples, where the phases mainly precipitated along the grain boundaries. Homogenous microstructure contributes to the higher wear resistance likely.

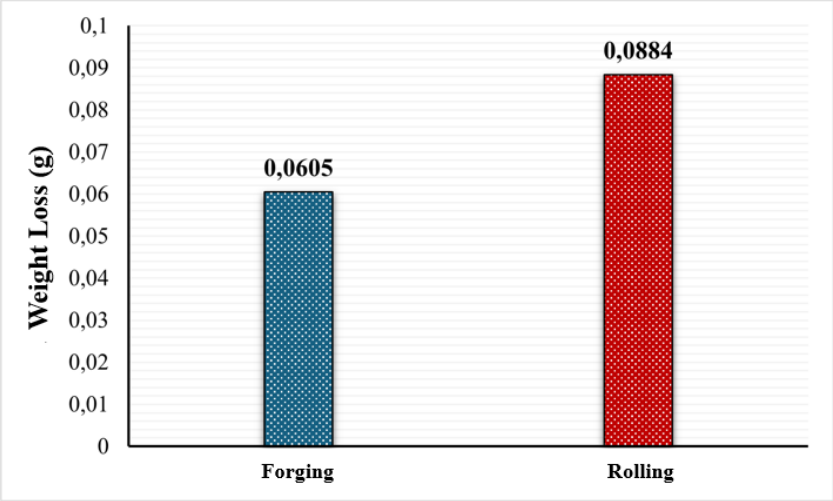

Figure 5. Weight loss results of CuCo1Ni1Be alloy formed by forging and rolling after wear test.

4. Conclusions

- The study revealed that different material properties were obtained at the same deformation ratio depending on the hot-forming method.
- It was observed that the alloy formed by rolling exhibited a finer microstructure compared to the alloy formed by forging and beryllite phases precipitate mostly at the grain boundaries in the alloy shaped by rolling compared to the alloy shaped by forging.
- The average grain size of the hot-forged alloy was 66.43 µm, while the average grain size of the rolled alloy was 21.83 µm. The average grain size decreased by 14.56% when using the rolling method compared to the forging method.
- The hardness of the alloy shaped by forging was 101.6 HRB, while the hardness of the alloy shaped by rolling was 97.8 HRB. It was determined that the hardness of the material increased by 3.74% with the forging method.
- The electrical conductivity of the alloy shaped by forging was measured as 25.3 MS/m, while the electrical conductivity of the alloy shaped by rolling was measured as 27.3 MS/m. The electrical conductivity of the material increased by 7.9% with the rolling method.
- The weight loss of the alloy formed by forging after the wear test was 0.0605 g and the weight loss of the alloy formed by rolling was 0.0884 g. It was determined that the weight loss increased by 46.12% in the rolling method compared to the forging method.
- It was determined that the forging method exhibited better mechanical and microstructural properties at low deformation rates. It is evaluated that a more homogeneous microstructure can be obtained and strength values can be improved with the rolling method at higher deformation rates.

- The research is ongoing and more results will be discussed.

5. References

[1] Elibol, Cagatay. "Effect of severe plastic deformation on the precipitation kinetics and the properties of CuCoNiBe alloys." Materials Today Communications 31 (2022): 103473.

[2] Zinkle, Steven J. "Evaluation of high strength, high conductivity CuNiBe alloys for fusion energy applications." Journal of Nuclear Materials 449.1-3 (2014): 277-289.

[3] Monzen, Ryoichi, Y. Shimada, and Chihiro Watanabe. "Mechanical properties of Cu-Ni-Be system alloys." Journal of Physics: Conference Series. Vol. 240. No. 1. IOP Publishing, 2010.

[4] Watanabe, Chihiro, and Ryoichi Monzen. "Precipitation process in a Cu-Ni-Be alloy." Solid State Phenomena 172 (2011): 432-436.

[5] Kızılaslan, Abdulkadir, and İbrahim Altınsoy. "The mechanism of two-step increase in hardness of precipitation hardened CuCoNiBe alloys and characterization of precipitates." Journal of Alloys and Compounds 701 (2017): 116-121.

[6] Ozgowicz, W., E. Kalinowska-Ozgowicz, and B. Grzegorczyk. "Thermomechanical treatment of low-alloy copper alloys of the kind CuCo2Be and CuCo1NiBe." Journal of Achievements in Materials and Manufacturing Engineering 46.2 (2011): 161-168.

[7]] Liao, Wanneng, et al. "Effect and mechanism of room temperature rolling, cryogenic rolling and heat treatment on mechanical properties and electrical conductivity of Cu-Ni-Si alloy with continuous directional solidification." Journal of Alloys and Compounds 949 (2023): 169748.

[8] Kulczyk, Mariusz, et al. "Improved compromise between the electrical conductivity and hardness of the thermo-mechanically treated CuCrZr alloy." Materials Science and Engineering: A 724 (2018): 45-52.

[9] Li, Zeng De, Chen Guang Lin, and Shun Cui. "Development of research and application of copper alloys with high strength and high conductivity." Advanced Materials Research 1053 (2014): 61-68.

[10] Çetinarslan, Cem S. "Effect of cold plastic deformation on electrical conductivity of various materials." Materials & design 30.3 (2009): 671-673.

DIMENSIONAL BEHAVIOR COMPARISON OF INJECTION MOLDED PA-6 AND PA-66

Meltem UZUNOGLU[1], Harun ZENGİN[2]

[1]Project Engineer, Ata Arms, m.uzunoglu@ataarms.com
[2]R&D Manager, Ata Arms, h.zengin@ataarms.com

ABSTRACT

Over the last few years, polymer science garnered significant attention. It has wide utilization areas like chemical industry, aerospace and defense industries. One of the polymeric materials is polyamide which has different types such as polyamide 6 (PA-6) and polyamide 66 (PA-66). Polyamide 6 (PA-6) and polyamide 66 (PA-66) are the majority of the commercial polyamide production and application due to superior properties such as high specific strength and stiffness, wear resistance, dimensional stability, low weight, and directional properties. They have different melting points, glass-transition temperatures, crystallinity, and tensile modulus. The properties of polymers can be enhanced with different fillers such as glass fibers (GF) and polymeric composite materials can be created. While those materials are technically well-known and widely used in the mentioned industries, test applications on actual part geometries documented in the literature are limited.

In this study, an actual industrial polymer part from the defense industry, which is a magazine of a weapon, is compared with different polymers and fiber contents, according to dimensional deformation after injection molding and hardness. PA6 and PA66 are used as polymeric materials. They are enhanced with glass fibers which have different concentrations such as %30 and %50. Plastic injection molding is used as the production process. During the injection molding, process parameters for instance melt temperature, injection speed, injection pressure is changed according to polymeric material. On the other hand; packing pressure, packing speed, cooling temperature and cooling time is not changed. Hardness and width of the magazine are examined as the polymeric material and composition of reinforcement (GF) change.

Keywords: Injection molding, production, polyamide, polymers, composite materials

1. INTRODUCTION

Polymer composites have an important influence on technical polymer usage. They have improved specific properties during the last twenty years [1]. The demand for polymeric composite materials increased due to their advanced properties, such as mechanical, thermal, and physical properties. Thus, they are usually used in automotive, aircraft, marine, and space structures [2].

Thermoplastic polymers have a wide variety of application areas in engineering, such as aircraft, automobiles, robots, machines, and rifle magazines, and can be used as matrix materials in composite materials. One of the thermoplastic polymers is polyamide, which has a high molecular weight, good solubility, specific strength, stiffness, wear resistance, dimensional stability, low weight, and directional properties when compared to conventional metallic materials [3].

Polyamide-6 (PA-6) is a semicrystalline polymer that has a wide range of properties. It has high stiffness and strength in dry conditions. Also, abrasion resistance, processability, chemical resistance, and electrical properties are excellent for the PA-6. It has high melting point, which is 220 °C. On the other

hand, it has high moisture absorption due to polarity of amide group [5], which limits its stability, stiffness, and strength [6].

Polyamide-66 (PA-66) has high thermal and mechanical properties. It can withstand higher temperatures, according to the other polyamides, and has a melting point of 265 °C. It absorbs less water than PA6 in a high-humidity environment [4].

Fillers modify the physical and structural properties of plastics [1]. High specific elastic modulus, tensile strength, chemical resistance, and low expansion rate and cost make glass fibers common reinforcements [3, 5]. There are important effects of the fibers in polyamide-6. They increase stiffness, tensile strength, creep resistance, fatigue strength, impact strength, anisotropy, and viscosity. On the other hand, they decrease thermal expansion coefficient, mold shrinkage, moisture pickup, ductility, and processability [7].

Injection molding is the most popular production process among plastics because it allows for the production of plastics with three-dimensional characteristics. It includes an injection unit and a clamp unit. In the injection unit, plastic is melted, and the melt is forced into the mold. The injection molding machine has a 50 to 1000-ton capacity, which is the maximum volume of melt that can be injected in a single cycle [6]. During injection molding process, dimensional deformation might occur according to material structure. Thus, material selection has significant role for injection molding production.

A toggle mechanism moves the mold during injection. And a hydraulic cylinder forces the screw forward, and the melt of the plastic goes into the mold. The screw turns to homogenize and pressurize the melt [6].

2. MATERIAL AND METHODS

In this study, composite materials are produced by plastic injection molding. Two different polymer matrices are used, which are Polyamide 6 (PA6) and Polyamide 6.6 (PA66) They are enhanced by glass fibers with different concentrations. These composites are produced by engineering plastics producer and their technical data is shown in Table1.

Table 1. Used Materials and Technical Data

Material Property	**Unit**	**PA6GF30**	**PA6GF50**	**PA66GF30**	**PA66GF50**
Product Code	**-**	M01000621	M01000166	M02000273	M02000343
Matrix Material	**-**	Polyamide 6 (PA-6)	Polyamide 6 (PA-6)	Polyamide 66 (PA-66)	Polyamide 66 (PA-66)
Glass Fiber Percentage	**%**	28 - 32	48 - 51	28 - 32	48 - 51
Density	**(g/cm³)**	1,30 – 1,34	1,53 – 1,56	1,35 – 1,37	1,52 – 1,54
Tensile Strength	**MPa**	115 - 125	200 - 220	170 - 180	180 -190
Tensile Strain at Break	**%**	> 2	2 - 4	2 - 5	< 3
Elastic Modulus	**MPa**	8000 - 9000	15000 - 16000	11000 - 12000	15000 - 16000

Izod Notched Impact Strength	**Kj/m²**	13 - 18	18 - 25	8 - 12	10 - 14
Melting Point	**°C**	225	225	260	265
References	**-**	[8]	[9]	[10]	[11]

Plastic injection molding machine is YIZUMI / UN160A5.

10 magazine is produced for each of the composite material by plastic injection molding, magazine figure shown in Figure 1.

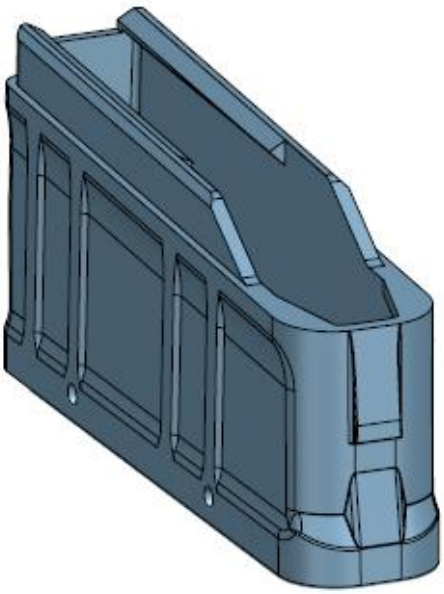

Figure 1. Magazine drawing

Dimension stability is examined for each sample according to Figure 2. below. There are two sides, the top and the bottom, of the magazine, and its dimensions can change during the process. Thus, each side is measured at 3 different points, which are the front, middle, and back. Nominal, theoretical dimensions are 9,75 for the top of the magazine and 17,3 for the bottom.

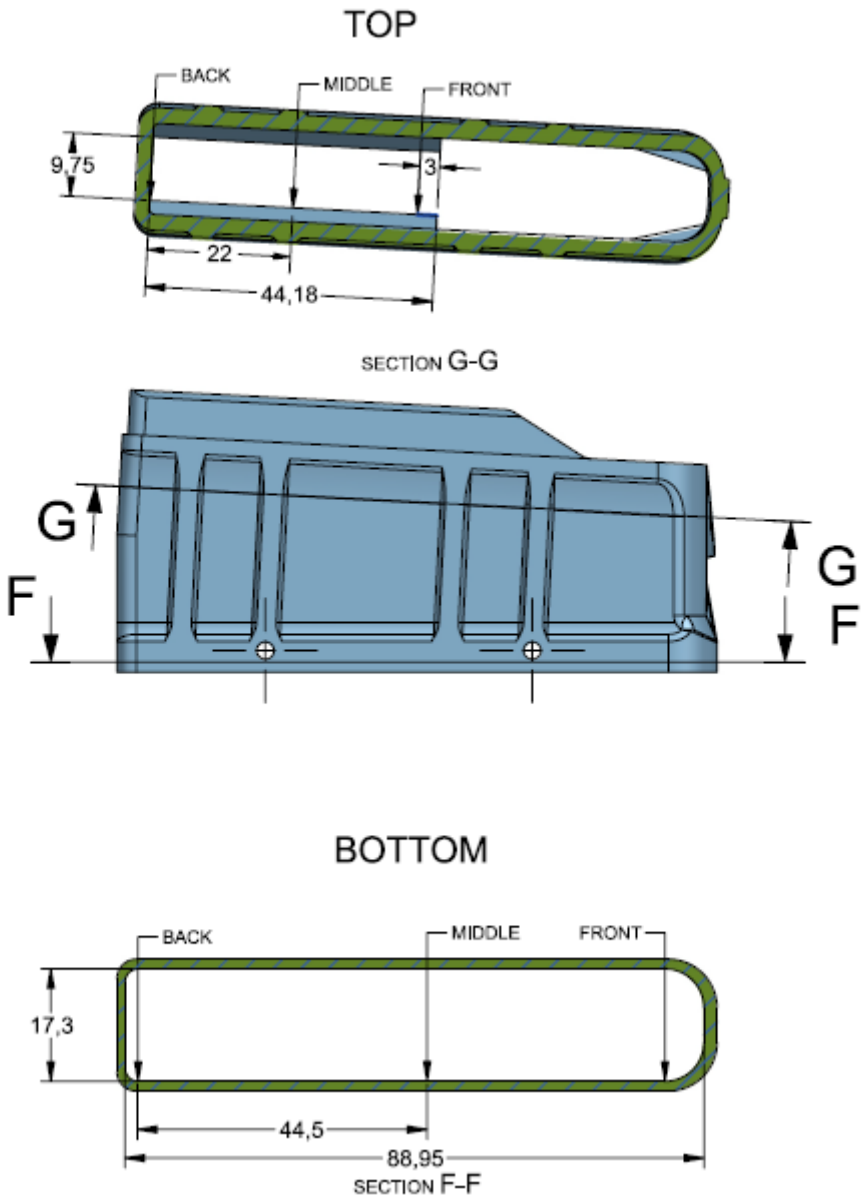

Figure 2. Location of measurements

For each material, hardness of 10 sample is measured with Shore D hardness and their average is calculated.

3. RESULTS AND DISCUSSION

Average of the 10 measurements for each magazine material are shown in the Table 3, dimensions are in mm scale.

Table 2. Average of the 10 different PA6GF30, PA6GF50, PA66GF30 and PA66GF50 samples

Location of Measurements		PA6GF30	PA6GF50	PA66GF30	PA66GF50
	Front	8,6745	8,8825	8,666	9,2395
Top	**Middle**	8,853	9,012	8,9035	9,263
	Back	9,7305	9,672	9,7015	9,74
	Front	17,1455	17,325	17,199	17,302
Bottom	**Middle**	16,4835	16,823	16,308	16,9635
	Back	17,3045	17,352	17,316	17,396

Top of the magazines is compared in the Figure 3 below.

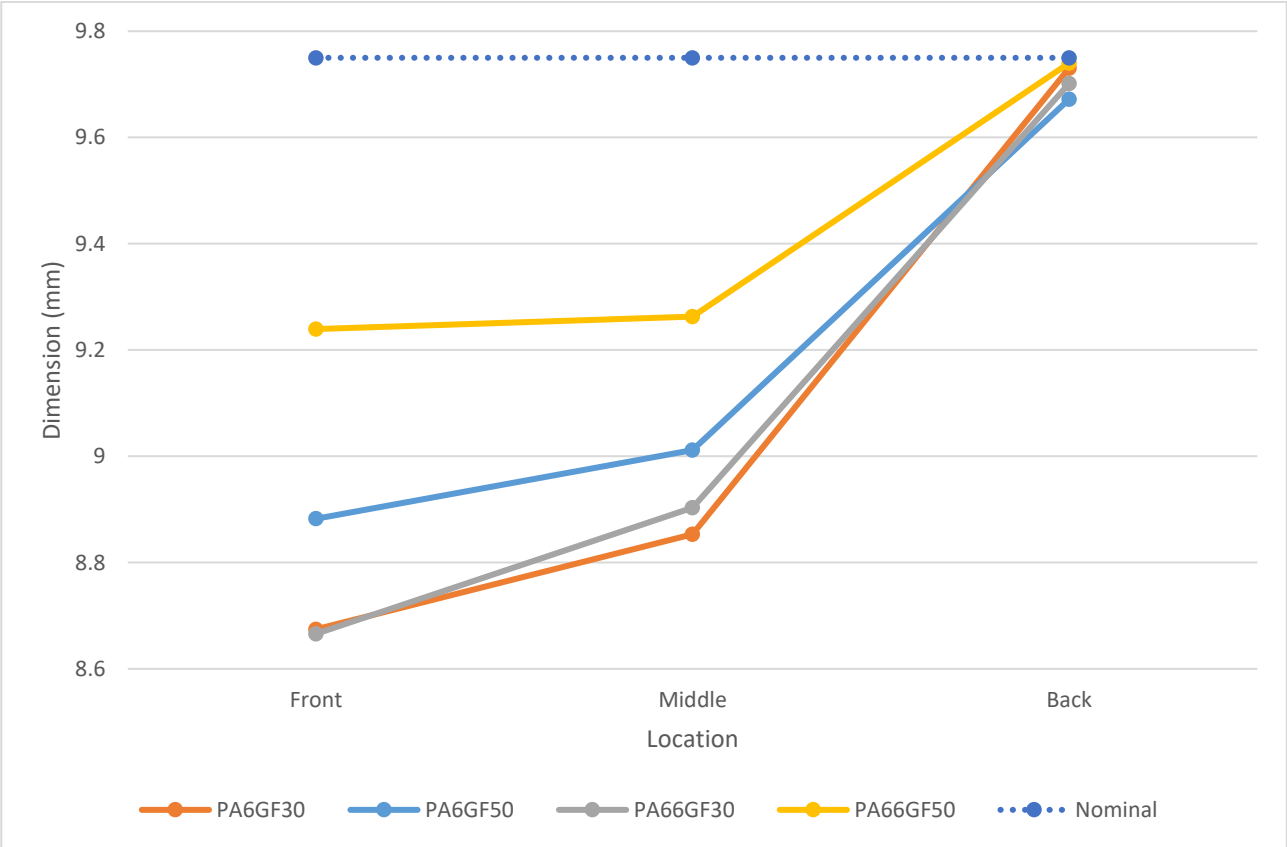

Figure 3. Measured dimensions for the top of the magazine

In the Figure 3, nominal width of the magazine is the theoretical dimension. All of the magazines have dimensional deformation. Highest shrinkage is at the front part of the top of the magazine. However,

increasing glass fiber concentration decreased the dimensional deformation. The best result is obtained from PA66GF50, which has the least deformation. Second preferred magazine is made of PA6GF50. However, as the glass fiber concentration decreased, dimensional deformation increased, and the width of the magazine decreased.

Bottom of the magazines is compared in the Figure 4 below.

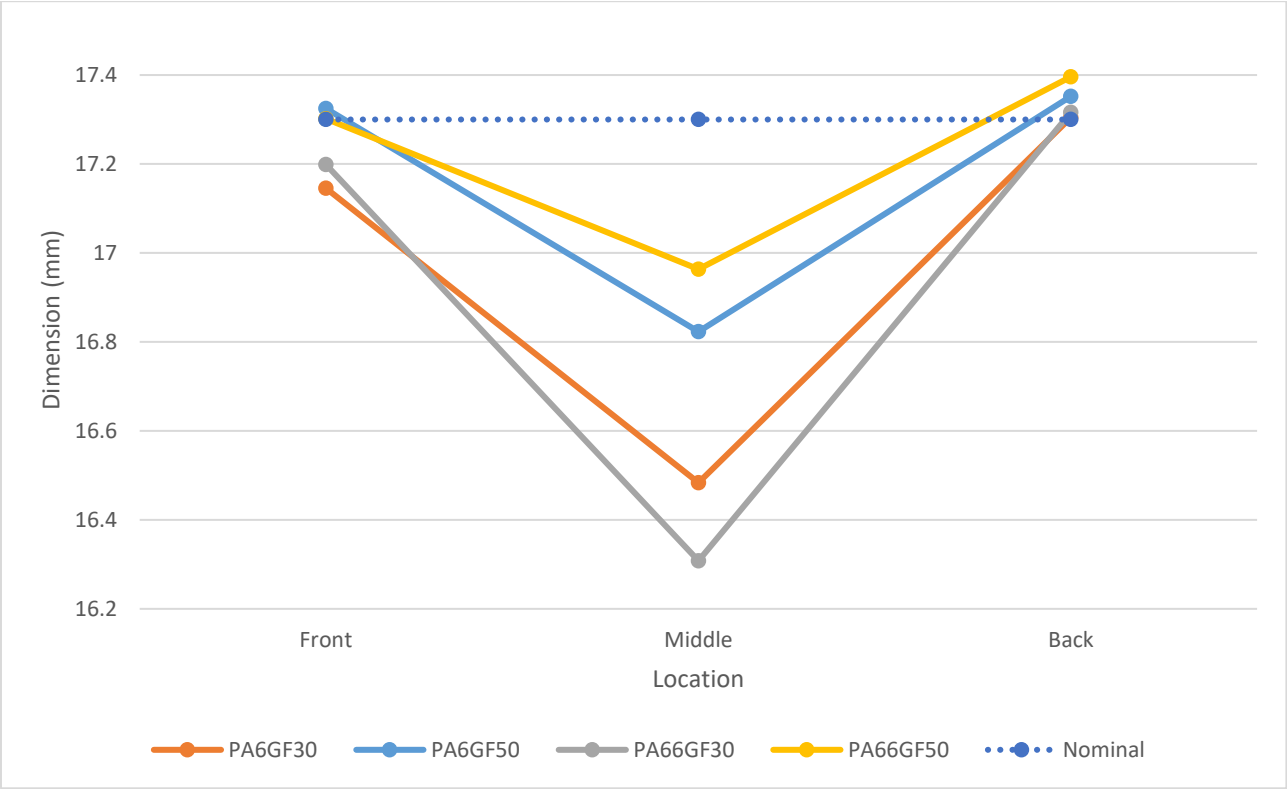

Figure 4. Measured dimensions for the bottom of the magazine

When the bottom part of the magazine is examined like the top part, it can be easily seen that the data taken form top and bottom of the magazine verifies itself. Highest shrinkage is at the middle part of the bottom of the magazine and PA66GF50 has the least dimensional deformation. The second preferred material is PA6GF50. The other two materials with 30% glass fiber are worse because the width of the magazine has decreased more.

The hardness values of the nanocomposite samples were measured by Shore-D in this study. 2 different samples for each composite material, and 10 different data points shown in Table 3 were taken for each magazine.

	PA6GF30		PA6GF50		PA66GF30		PA66GF50	
Measurement No:	**Sample 1**	**Sample 2**	**Sample 1**	**Sample 2**	**Sample 1**	**Sample 2**	**Sample 1**	**Sample 2**
1	75	78	79	78	80	81	82	82
2	77	77	81	80	81	82	83	81
3	79	77	81	78	78	82	81	82
4	78	78	78	73	80	82	84	78
5	77	77	81	80	79	79	82	82
6	79	76	81	79	82	83	83	82
7	79	78	81	81	82	82	85	82
8	80	76	81	81	82	81	85	79
9	80	79	79	81	81	78	83	82
10	79	78	80	79	83	82	85	80
Average Value:	78,3	77,4	80,2	79	80,8	81,2	83,3	81

The table is summarized with the average data in Figure5.

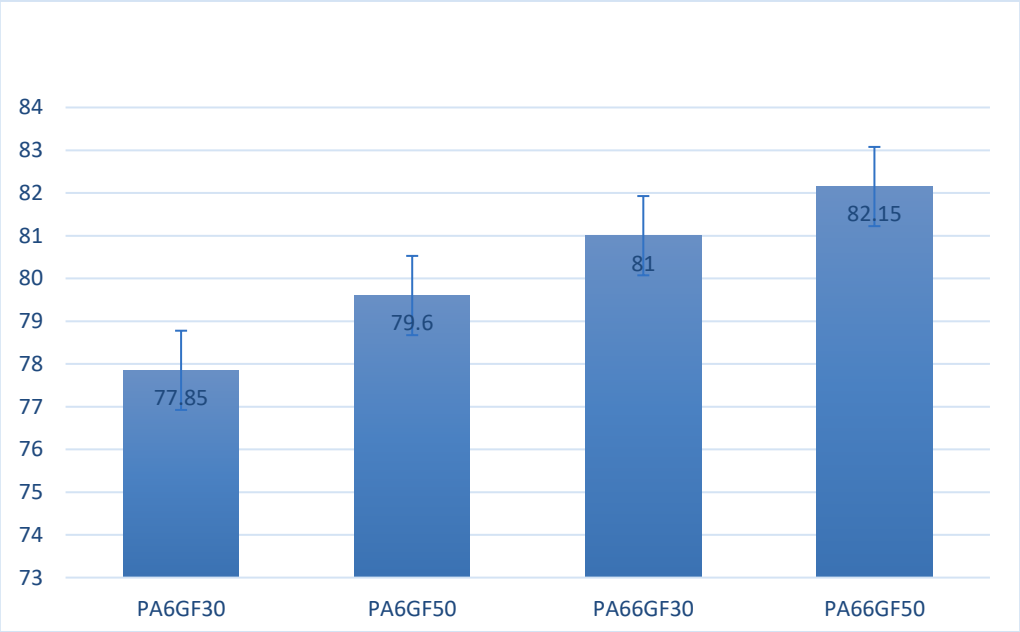

Figure 5. Shore D Hardness Data

According to this data, hardest material is PA66GF50 and the second one is PA66GF30. Hardness is mainly affected by polymeric material.

4, CONCLUSION

The best dimensional stability is obtained from PA66GF50 and PA6GF50 samples. This result shows that increasing fiber content reduces the dimensional deformation. This verified the information in literature that is fiber addition decrease the mold shrinkage. If dimensional stability is important depending on the area of use, it is better to use materials with high fiber content due to low shrinkage. Difference between the best and the worst result for the top and the bottom of the magazine is %3,32 and %1,62 respectively. This shows that shrinkage is more at the top of the magazine.

On the other hand, fiber addition has little influence on hardness by comparison to the dimensional stability. However, if hardness is compared in the same polymeric matrix material, fiber addition increased the hardness. And also, when polymeric matrix materials are compared, PA66 has higher hardness than PA6.

ACKNOWLEDGEMENTS

This work was supported by Ata Arms company.

REFERENCES

1. Adam Gnatowski, Influence Of Injectıon Mouldıng Condıtıon And Annealıng On Thermal Propertıes, Structure, Color And Gloss Of Composıte Polyamıde 6 Wıth Glass Beads, Composites Theory and Practice, 2012

2. Emel Kuram, Micro-machinability of injection molded polyamide 6 polymer and glass-fiber reinforced polyamide 6 composite, 2015

3. V, N, Gaitonde, S, R, Karnik, Francisco Mata, J, Paulo Davim, Modeling and Analysis of Machinability Characteristics in PA6 and PA66 GF30 Polyamides through Artificial Neural Network, 2010

4. R, Rulkens, C, Koning, Chemistry and Technology of Polyamides, 2012

5. Lin, Y., Zhong, W., Shen, L., Xu, P., & Du, Q. (2005). Study on the Relationship Between Crystalline Structures and Physical Properties of Polyamide-6. Journal of Macromolecular Science, Part B, 44(2), 161–175.

6. Cahit Can Cansever, Effects of Injection Molding Conditions on the Mechanical Properties opf Polyamide / Glass Fiber Composites, Master Thesis, Middle East Technical University, 2007

7. D, Hull, T, W, Clyne, An Introduction to Composite Materials, 1996

8. Tisan, M01000621, Teknik Bilgi Formu, Tislamid

9. Tisan, M01000166, Teknik Bilgi Formu, Tislamid

10. Tisan, M02000273, Teknik Bilgi Formu, Tislamid

11. Tisan, M02000343, Teknik Bilgi Formu, Tislamid

SAVUNMA SANAYİNDE ZIRH, KORUMA VE GÖRÜNMEZLİK TEKNOLOJİLERİ

Almıla Gökçe DAL[1] İzel YUMAK[2],
[1]Askeri ArGe Tasarım Uzmanı, Koluman Otomotiv Endüstri A.Ş. almila.dal@koluman.com
[2] Askeri Satın Alma Uzmanı, Koluman Otomotiv Endüstri A.Ş. izel.yumak@koluman.com

Özet

Savunma sanayinde zırh, koruma ve görünmezlik teknolojileri, askeri araçlar, personel ve askeri tesislerin güvenliği için önemli bir rol oynamaktadır. Bu teknolojiler, askeri güçlerin operasyonel yeteneklerini artırmak ve askeri personelin güvenliğini sağlamak amacıyla sürekli olarak geliştirilmektedir.[6] Zırh teknolojileri, bireylerin ve araçların düşman tehditlerinden korunması için tasarlanmış malzemeleri ve sistemleri kapsar. Geleneksel zırh malzemeleri arasında çelik, seramik ve kompozitler bulunur. Koruma teknolojileri, zırhın yanı sıra çeşitli savunma ve güvenlik sistemlerini içerir. Bu teknolojiler arasında balistik kasklar, vücut zırhı, patlayıcı maddelere karşı koruyucu giysiler ve anti-mayın ayakkabıları yer alır. Araçlar için geliştirilen aktif koruma sistemleri, tehditleri algılayarak otomatik olarak savunma mekanizmalarını devreye sokar. Görünmezlik teknolojileri, düşman radar ve sensörlerinden saklanmak amacıyla kullanılan ileri düzey teknolojilerdir. Bu alanda en bilinen yöntemlerden biri, radar dalgalarını soğuran ve yansıtan özel kaplamalardır.

Anahtar kelimeler: Savunma sanayinde zırh, zırh teknolojisi, koruma teknolojileri, görünmezlik, görünmezlik teknolojileri.

Abstract

In the defense industry, armor, protection and visibility technologies play an important role in the security of military vehicles, personnel and military facilities. This technology is constantly being developed with the aim of increasing military strength and increasing the amount of military power.Armor technologies encompass materials and systems designed to shield individuals and vehicles from enemy threats. Traditional armor materials include steel, ceramics, and composites. Protection technologies encompass various defense and security systems in addition to armor. These technologies include ballistic helmets, body armor, protective clothing against explosive materials, and anti-mine shoes. Active protection systems developed for vehicles automatically engage defense mechanisms by detecting threats. Invisibility technologies are advanced methods utilized to conceal from enemy radars and sensors. One of the most well-known methods in this field involves specialized coatings that absorb and deflect radar waves.

Keywords: In the defense industry, Armor, Armor technology, Protection technologies, Invisibility, Invisibility technologies.

1. GİRİŞ

Zırh, koruma ve görünmezlik teknolojileri, askeri ve güvenlik alanlarında kritik öneme sahip gelişmelerdir. Bu teknolojiler, modern savaş alanlarında ve güvenlik uygulamalarında personel ve ekipmanların korunması amacıyla kullanılır. Bu makalede, zırh, koruma ve görünmezlik teknolojilerinin

gelişimi, kullanım alanları ve gelecekteki potansiyelleri ele alınacaktır. Ayrıca, bu teknolojilerin etkinliğini artırmak için yapılan araştırmalar ve geliştirmeler de incelenecektir.

2. MALZEME VE YÖNTEM

Zırh Teknolojileri

Zırh teknolojileri, bireylerin ve araçların düşman tehditlerinden korunması için tasarlanmış malzemeleri ve sistemleri kapsar. Geleneksel zırh malzemeleri arasında çelik, seramik ve kompozitler bulunur. Dünya ve yerli kullanım oranlarını Şekil.1 de görebilirsiniz.

Zırh Malzemesi	Dünya Kullanım Oranı (%)	Yerli Kullanım Oranı (%)	Kullanım Alanları	Avantajları
Çelik	45	50	Ağır zırhlı araçlar, tanklar	Yüksek mukavemet, düşük maliyet
Seramik	30	25	Kurşun geçirmez yelekler, hafif zırhlı araçlar	Hafiflik, yüksek sertlik, balistik koruma
Kompozit	25	25	Askeri araçlar, kişisel koruma ekipmanları	Hafiflik, enerji emici özellikler

Şekil 1. Zırh Malzemelerinin Dünya ve Yerli kullanım Oranları

Çelik Zırh: Yüksek mukavemeti ve dayanıklılığı ile bilinen çelik zırh, özellikle ağır zırhlı araçlarda kullanılır. [1] Çelik, düşük maliyeti ve kolay üretilebilirliği nedeniyle tercih edilmektedir. Çelik zırhın mukavemetini artırmak için, çeşitli alaşımlar ve ısıl işlemler kullanılarak mikro yapısında değişiklikler yapılmaktadır.

Seramik Zırh: Seramik zırh bkz. Şekil.2 daha hafif olup balistik tehditlere karşı etkili bir koruma sağlar [1].Seramik malzemeler, yüksek sertlikleri ve düşük yoğunlukları sayesinde, mermileri dağıtarak ve enerjisini emerek etkili bir koruma sağlar. Alümina, bor karbür (Güvenlik güçlerini korumak için üretilen kurşun geçirmez yeleklerde bor karbür kullanılabilir) ve silisyum karbür gibi seramik malzemeler yaygın olarak kullanılmaktadır.

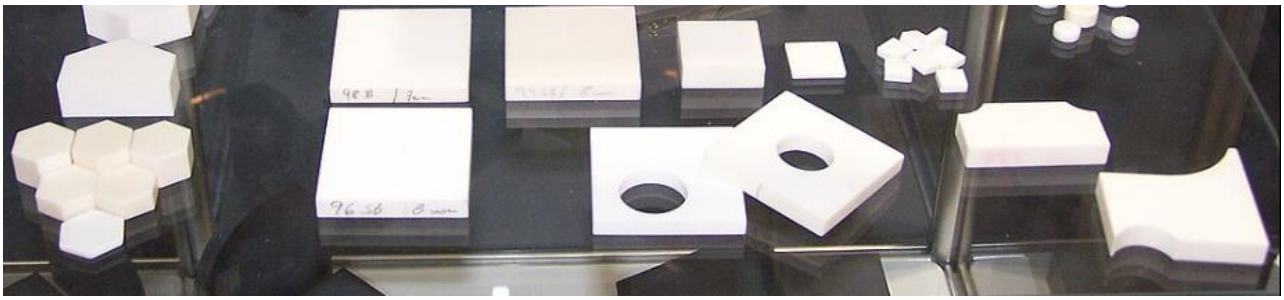

Şekil 2. Seramik Zırh

Kompozit Zırh: Kompozit zırhlar, farklı malzemelerin bir araya getirilmesiyle hem mukavemet hem de hafiflik açısından üstün koruma sunar [1]. Karbon fiber, kevlar ve polietilen gibi malzemeler, kompozit zırhların üretiminde kullanılmaktadır. Bu malzemeler, enerji emici özellikleri sayesinde balistik tehditlere karşı yüksek koruma sağlar. Kompozit zırh koruma uygulamaları için üstün hafif malzeme - temel bir seramik kompozit zırh sistemi, benzer çelik tabanlı sistemlerin ağırlığının yaklaşık yarısı kadardır.

Koruma Teknolojileri

Koruma teknolojileri, zırhın yanı sıra çeşitli savunma ve güvenlik sistemlerini içerir. Bu teknolojiler arasında balistik kasklar, vücut zırhı, patlayıcı maddelere karşı koruyucu giysiler ve anti-mayın ayakkabıları yer alır.

Balistik Kasklar ve Vücut Zırhı: Balistik kasklar bkz. Şekil.3 vücut zırhı, askeri personelin hayatta kalma şansını artırmak ve operasyonel etkinliklerini korumak amacıyla geliştirilmiştir [2]. Bu ekipmanlar, genellikle kevlar, dyneema ve seramik plakalar gibi yüksek mukavemetli malzemelerden yapılmaktadır.

Şekil 3. Balistik Kask

Koruyucu Giysiler: Patlayıcı maddelere karşı koruyucu giysiler, askeri personeli patlama şok dalgalarından ve şarapnellerden korur. Bu giysiler, genellikle kalın kevlar tabakalar ve balistik naylon gibi malzemelerden üretilmektedir. bkz. Şekil.4

Şekil 4. Koruyucu Giysi

Aktif Koruma Sistemleri: Araçlar için geliştirilen aktif koruma sistemleri, tehditleri algılayarak otomatik olarak savunma mekanizmalarını devreye sokar [2]. Bu sistemler, radar ve sensörler kullanarak yaklaşan tehditleri tespit eder ve patlayıcı mermiler veya elektromanyetik darbeler ile tehditleri etkisiz hale getirir.

Görünmezlik Teknolojileri

Görünmezlik teknolojileri, düşman radar ve sensörlerinden saklanmak amacıyla kullanılan ileri düzey teknolojilerdir. Bu alanda en bilinen yöntemlerden biri, radar dalgalarını soğuran ve yansıtan özel kaplamalardır [3].

Stealth Teknolojisi: Stealth teknolojisi, özellikle hava araçları ve gemilerde bkz. Şekil.5 yaygın olarak kullanılır. Bu teknoloji, radar yansımalarını minimize ederek düşman radarlarının tespit etme olasılığını azaltır. Stealth kaplamalar, radyo dalgalarını soğurarak ve yansıtarak nesneleri görünmez kılar.

Şekil 5. Stealth teknolojisine uygun gemi

Optik Kamuflaj: Optik kamuflaj teknolojileri, ışığı bükerek veya yansıtarak nesneleri görünmez kılma hedefindedir. Metamalzemeler kullanılarak geliştirilen bu teknolojiler, nesnelerin etrafındaki ışığı manipüle ederek görünmezlik sağlar. Bu teknolojiler, askeri operasyonlarda büyük bir avantaj sağlayarak düşmanın fark etme süresini uzatır ve saldırı riskini azaltır [4].

3. SONUÇLAR VE TARTIŞMA

Zırh, koruma ve görünmezlik teknolojilerindeki yenilikler, güvenlik ve askeri stratejilerde önemli değişikliklere yol açmaktadır. Bu teknolojiler, modern savaş alanlarında ve güvenlik uygulamalarında personel ve ekipmanların korunmasında hayati bir rol oynamaktadır [5]. Çelik, seramik ve kompozit zırhlar, farklı tehditlere karşı etkili koruma sağlarken, balistik kasklar ve vücut zırhları askeri personelin hayatta kalma şansını artırmaktadır [1]. Ayrıca, aktif koruma sistemleri ve optik kamuflaj gibi ileri teknolojiler, askeri operasyonlarda büyük avantajlar sağlamaktadır [4].
Nanoteknoloji ve metamalzemeler gibi gelişen malzeme bilimleri, zırh ve koruma teknolojilerinin etkinliğini artırmak için yeni çözümler sunmaktadır. Örneğin, karbon nanotüplerin zırh sistemlerinde kullanılması, daha hafif ve dayanıklı zırhların üretilmesini mümkün kılmaktadır [4]. Aynı şekilde, metamalzemeler ile geliştirilen görünmezlik teknolojileri, askeri araçların ve personelin düşman radarlarından saklanmasını sağlamaktadır [4].
Metamalzemeler negatif kırılma bkz. Şekil.5 indisine sahip yüzeylerin elde edilmesine, yani gönderilen ışığın beklenenin aksi bir yönde kırıldığı bir ortamın oluşmasına olanak sağlar.

Şekil 5. Negatif Kırılma

4. SONUÇ, TARTIŞMA VE ÖNERİLER

Gelecekte, zırh, koruma ve görünmezlik teknolojilerinin daha da gelişmesi beklenmektedir. Bu alanda yapılacak araştırmalar ve geliştirmeler, askeri ve güvenlik uygulamalarında önemli yeniliklere yol açacaktır. İşte bu alandaki bazı öneriler:

Malzeme Araştırmaları: Yeni malzemelerin keşfi ve mevcut malzemelerin geliştirilmesi, zırh ve koruma teknolojilerinin etkinliğini artıracaktır. Özellikle nanoteknoloji ve metamalzemeler üzerine yapılacak araştırmalar, bu alanda önemli ilerlemeler sağlayabilir.

Entegre Sistemler: Zırh ve koruma teknolojilerinin entegre edilmesi, askeri personelin ve araçların korunmasında daha etkili çözümler sunacaktır. Örneğin, aktif koruma sistemlerinin ve pasif zırhların birleştirilmesi, tehditlere karşı daha kapsamlı bir koruma sağlayabilir.

Eğitim ve Uygulama: Askeri personelin yeni zırh ve koruma teknolojileri konusunda eğitilmesi, bu teknolojilerin etkin kullanımını sağlayacaktır. Ayrıca, bu teknolojilerin saha testleri ve simülasyonlar ile sürekli olarak değerlendirilmesi, performanslarının optimize edilmesine katkı sağlayacaktır.

Çevre Dostu Malzemeler: Sürdürülebilir ve geri dönüştürülebilir malzemelerin kullanımı, zırh ve koruma teknolojilerinin çevresel etkilerini azaltacaktır. Bu alanda yapılacak çalışmalar, askeri operasyonların doğa dostu olmasına katkı sağlayacaktır.

5. KAYNAKLAR

[1] Aksoy, M. (2017). “Stealth Teknolojisi ve Uygulamaları.” Havacılık ve Uzay Teknolojileri Dergisi, 10(1), 34-47.
[2] Çelik, T. (2019). “Modern Zırh Sistemleri ve Uygulamaları.” Savunma Teknolojileri Dergisi, 12(3), 45-57.
[3] Demir, H. (2021). “Nanoteknoloji ile Geliştirilen Yeni Nesil Koruma Sistemleri.” Teknolojik Yenilikler ve Güvenlik, 8(4), 203-216.
[4] Kaya, E. (2018). “Görünmezlik Teknolojilerinin Geleceği.” Askeri Bilimler ve Strateji Araştırmaları Dergisi, 5(1), 89-101.
[5] Yıldırım, S. (2020). “Balistik Koruma ve Malzeme Bilimi.” Mühendislik ve Teknoloji, 15(2), 112-124.
[6] Smith, John. "The Importance of Education." Education Journal, 2021, 3, 45-56.

ÖZET SUNUMLAR

ROUGHNESS AND MICROSTRUCTURE CHARACTERIZATION OF AISI 316L LASER-POWDER BED FUSION SPECIMENS AFTER APPLYING A VIBRATION-ASSISTED BALL BURNISHING PROCESS

Eric Velázquez-Corral[1], Adrián Travieso-Disotuar[1,2], Ramón Jerez-Mesa[1], Montserrat Vilaseca[2], Clément Keller[3] and Gilles Dessein[3]

[1]Mechanical Engineering Department, Universitat Politècnica de Catalunya, Av.Eduard Maristany 10-14, Barcelona, 08019, Spain, eric.velazquez.corral@upc.edu; adrian.alberto.travieso@upc.edu; ramon.jerez@upc.edu
[2]Eurecat, Centre Tecnològic de Catalunya, Unit of Metallic and Ceramic Materials, Plaça de la Ciència, Manresa, Barcelona, 08243, Spain, montserrat.vilaseca@eurecat.org
[3]Laboratoire Génie de Production, Université de Technologie Tarbes Occitanie Pyrénées, 47 Avenue d'Azereix, Tarbes, 65000, Occitanie, France, clement.keller@uttop.fr; gilles.dessein@uttop.fr

Abstract

The objective of this study is to analyze the effect of adding an ultrasonic vibration assistance within a ball burnishing (VABB) process onto cylindrical AISI 316L laser powder bed fusion (LPBF) specimens. The purpose of the specimens is to improve surface integrity, in terms of roughness reduction and microstructure reconstruction, to optimize the fatigue performance for testing samples according to ISO 1099:2017, reducing surface imperfections with burnishing. All printed specimens were manufactured in the Z direction using a laser power of 195W, a scanning speed of 900 mm/s, a hatch distance of 0.1 mm, a layer thickness of 40 µm, and a scan angle of 67°. The preliminary experimental campaign is based on a full factorial design of 3 variables (burnishing force, number of passes, and BB/VABB) with 2 levels for each. It was found that the estimated depth of affectation is 4-5 µm and 5-7 µm, for BB and VABB respectively, thus demonstrating the positive effect of the vibration assistance. The softening effect while deforming, caused by the vibration assistance, helped to reconstruct the surface, obtaining higher depths of affectation. In terms of topology, the surface average roughness for all specimens is within the range of 0.2-0.4 µm, showing an improvement of 74% in the best case compared to the machined surface. The material distribution parameters, Skewness and Kurtosis, show an almost perfect Gaussian distribution for all the specimens analyzed.

***Keywords*:** Laser powder bed fusion, Ball burnishing, Surface integrity

MYCOREMEDIATION OF HEAVY METAL POLLUTION: A REVIEW

Cazan Bogdan[1], Iordache Ovidiu-George[1], Mihai Carmen[1], Perdum Elena[1], Dinca Laurentiu[1]

[1]National Research and Development Institute for Textiles and Leather, Lucretiu Patrascanu 16, Bucharest, Romania, e-mail: bogdan.cazan@incdtp.ro
[1]National Research and Development Institute for Textiles and Leather, Lucretiu Patrascanu 16, Bucharest, Romania, e-mail: ovidiu.iordache@incdtp.ro
[1]National Research and Development Institute for Textiles and Leather, Lucretiu Patrascanu 16, Bucharest, Romania, e-mail: carmen.mihai@incdtp.ro
[1]National Research and Development Institute for Textiles and Leather, Lucretiu Patrascanu 16, Bucharest, Romania, e-mail: elena.perdum@incdtp.ro
[1]National Research and Development Institute for Textiles and Leather, Lucretiu Patrascanu 16, Bucharest, Romania, e-mail: laurentiu.dinca@incdtp.ro

Abstract
Heavy metal pollution of the environment is one of the biggest issues of today's society. Whether it affects soils or water, once introduced in the environment, heavy metals cannot be biodegraded. In agriculture, heavy metal pollution affects both the quality and the quantity of the crops. In the aquatic environment, heavy metals affects not only the aquatic life but also it affects human directly, through the contamination of the drinking water. Their presence in environment results in bioaccumulation, further affecting biological and ecological cycles. Mining activities, chemical weathering of minerals, leather and textile industry and industrial discharges are just a few examples of heavy metals pollution sources. However, some heavy metals have importance as trace elements, for the growth and development of organisms such as plants and fungi. Due to their persistence in environment, microorganisms have evolved mechanisms to tolerate heavy metals presence through adsorption or chemical reduction of metal ions. In fact, the role of fungi as decomposers in the ecosystems led to the studying of their enzymes and ability to mycoremediate heavy metals. To obtain mycoremediation of heavy metal pollution, the aim is to determinate the right fungal species to target a specific pollutant. This paper aims to review the potential of fungi to bioremediate heavy metal pollution.

Keywords: mycoremediation, bioaccumulation, fungi, heavy metal pollution, environment

GANODERMA LUCIDUM LEATHER AS A SUSTAINABLE ALTERNATIVE POTENTIAL FOR FASHION INDUSTRY

Cazan Bogdan[1], Iordache Ovidiu-George[1], Mihai Carmen[1], Perdum Elena[1], Dinca Laurentiu[1]

[1]National Research and Development Institute for Textiles and Leather, Lucretiu Patrascanu 16, Bucharest, Romania, e-mail: bogdan.cazan@incdtp.ro

[1]National Research and Development Institute for Textiles and Leather, Lucretiu Patrascanu 16, Bucharest, Romania, e-mail: ovidiu.iordache@incdtp.ro

[1]National Research and Development Institute for Textiles and Leather, Lucretiu Patrascanu 16, Bucharest, Romania, e-mail: carmen.mihai@incdtp.ro

[1]National Research and Development Institute for Textiles and Leather, Lucretiu Patrascanu 16, Bucharest, Romania, e-mail: elena.perdum@incdtp.ro

[1]National Research and Development Institute for Textiles and Leather, Lucretiu Patrascanu 16, Bucharest, Romania, e-mail: laurentiu.dinca@incdtp.ro

Abstract

Leather demand in fashion industry has increased in the recent years, making it more difficult for the leather producers to provide the needed quantity. This matter led to an increase in the number of the livestock farms thus creating other environmental issues as water pollution, deforestation, overgrazing and gas emissions. Beside this, the processing of animal hides into leather requires extra steps that involves toxic chemicals which eventually will get released into the environment. In this regard, one of the solutions we aimed for was the production of fungi leather. Fungi leather requires less water and surface to grow, being obtained through the upcycling of agricultural and forestry waste and by-products, using fungal growth process. There is a wide range of filamentous fungi that can be used for this process, highest yield ones being wood-decaying fungi or white rot fungi from genres *Polyporus sp.*, *Ganoderma sp.*, *Trametes sp.*, *Pleurotus sp.*, *Fomes sp.*. This study focused mainly on the *Ganoderma lucidum* strain and on the production of pure mycelium mats. Pure mycelium mats obtained this way can adopt multiple properties and show promising as substitutes for present petrochemically produced materials or animal leather. The process we used is divided in chemical and physical treatment. The main methods used in chemical treatment were deacetylation of chitin and the cross-linking of chitosan. Following cross-linking the pure mycelium mat (PMM) was subjected to a plasticizer agent. In the end, after physical treatment a minimum viable product was obtained.

Keywords: fungi leather, *Ganoderma lucidum*, mycomaterial, upcycling, mycelium, biodegradable

SEÇİCİ LAZER ERGİTME YÖNTEMİ İLE ÜRETİLEN AlSi10Mg ALAŞIMLARIN KRİYOJENİK İŞLEMİ

Pelin SEZER[1], Semra KURAMA[2] Taner KARAGÖZ[3]

[1]Eskişehir Osmangazi Üniversitesi, Metalurji ve Malzeme Mühendisliği, pelin.sezer@ogu.edu.tr
[2]Eskişehir Teknik Üniversitesi, Malzeme Bilimi ve Mühendisliği, skurama@eskisehir.edu.tr
[3]Coşkunöz Holding, Ar-Ge Departmanı, tkaragoz@coskunoz.com.tr

Özet
AlSi10Mg alaşımları, otomotiv, havacılık ve savunma sanayi endüstrilerinde hafiflik ve üstün termal özellikler ile mekanik özelliklerin bir arada olması gerektiği uygulamalarda önemli bir yere sahiptir. Dökülebilirliği ve işlenebilirliği sayesinde de sanayi için üretimde kolaylık sağlayan bir alaşım olarak karşımıza çıkmaktadır. Bunun yanında, Eklemeli İmalat (Eİ) teknolojilerindeki hızlı ilerlemeler, çevre dostu ve ekonomik olarak uygun maliyetli yeni alaşımların üretimini teşvik etmiştir. Seçici Lazer Ergitme (SLE), karmaşık yapıların üretilmesinde büyük avantaj sağlayan bir eklemeli imalat teknolojisidir ve topolojik olarak optimize edilmiş yapılarla hafif parçaların üretimine imkan sağladığı bilinmektedir. Tüm bu avantajlarının yanında katmanlı üretim teknolojisiyle ilgili çalışmalarda ısıl işlem gibi post-process adı verilen son işlem gereksinimleri endüstride ve literatür çalışmalarında önemini korumaktadır. AlSi10Mg alaşımı üzerinde olumlu etkileri olduğu belirtilen kriyojenik işlemin genellikle özel ısıl işlem süreçleri gerektiğinde tercih edilebildiği belirtilmektedir. Bu çalışmada, SLE yöntemi kullanılarak üretilen AlSi10Mg alaşım malzemesinin kriyojenik işlem etkisinin mekanik özelliklere etkisi incelenmiştir. SLE üretim parametreleri 700W gücünde çift lazerle 60 µm katman kalınlığında, şerit (stripe) tarama stratejisi olarak belirlenmiş ve blok parça üretimi gerçekleştirilmiştir. Blok üretiminden sonra ASTM E8/8M standardına göre çekme testi numuneleri çıkarılmıştır. Kriyojenik işlem -196°C sıcaklıkta, 24 ve 36 saatlik işlem sürelerinde uygulanmıştır. Bu işlemin ardından, numunelere çekme ve sertlik testleri yapılmış ve mekanik özellikleri bu testler üzerinden incelenmiştir. Sonuçlar, kriyojenik işlem uygulanan numunelerin sertliklerinin işlem görmemiş halleriyle karşılaştırıldığında, 36 saatlik döngü sonrasında arttığını, ancak 24 saatlik döngü sonrasında azaldığını ortaya koymuştur. Kriyojenik işlem süresindeki değişimlerin büyük farklılıklara yol açmadığı gözlemlenirken işlem süresi arttıkça yüzde uzama değerleri artarken, çekme ve akma mukavemeti değerleri 24 saatlik işlem gören numunelerde daha yüksek bulunmuş ve 36 saat işlem gören numunelerde hafif bir düşüş yaşanmıştır. Sonuç olarak, kriyojenik işlemin SLE ile üretilen AlSi10Mg numunelerinin sertliğinde önemli bir değişim yaratmamakla birlikte, çekme mukavemeti, akma mukavemeti ve uzama yüzdesi değerlerinde anlamlı etkiler gösterdiği söylenebilir.

Anahtar Kelimeler: Eklemeli İmalat, Seçici Lazer Ergitme, Kriyojenik İşlem, Alüminyum alaşımları, AlSi10Mg

SOFTWARE APPROACHES AND METALLURGICAL CHARACTERIZATION IN THE CASTING PRODUCTION OF 2-PIECE BALL VALVES

Sezer Hivda ÖZDEN[1], Ozan ÇOBAN[2]

[1]Gedik Termo Vana Tic. Ve San. A.Ş., Sakarya, Türkiye
[2]Istanbul Gedik University Gedik Vacational School, Machinary and Metal Technologies Department, Istanbul, Türkiye

sezer.ozden@gedik.com.tr, ozan.coban@gedik.edu.tr

Abstract
This study focuses on the production of two-piece ball valves, used in petrochemical, made from lamellar graphite cast iron, industry conforming to the ASTM A216 WCB standard, which specifies steel castings suitable for fusion welding in high-temperature services. The primary manufacturing technique employed is casting, followed by precision machining processes. To meet the dimensional requirements specified by API 6D for end-to-end length, and to ensure minimum wall thickness and flange diameter according to ASME 16.34 and ASME 16.5 for various pressure classes, initial castings are machined to achieve the final desired specifications.
Significant advancements in software design and flow analysis within the casting processes have been incorporated in this study, enhancing the production quality of cast materials with designated machining allowances. The cast materials underwent rigorous metallurgical evaluations, including non-destructive testing, hardness testing, tensile testing, impact testing, and microstructural characterization, to ensure material integrity and performance.
Furthermore, comprehensive testing protocols, such as shell tests and leak tests conforming to API 6D and API 598 standards, were conducted to assess the body strength and verify the operational performance of the assembled valves. These measures ensured that the valves met the stringent requirements for durability and functionality in high-temperature and high-pressure environments. This integrated approach of advanced casting techniques, precise machining, and thorough testing underscores the technical robustness of the valve production process.

Keywords: API, Casting, Valve, Machining, Software Design

ÖZEL KAFA ALTI PUNTALI KAYNAK FORMLU PERÇİN TASARIMI VE SİMÜLASYON DESTEKLİ ÜRETİMİ

Aslıhan KALYON[1], Alper BAYGUT[2], Yener YILMAZ[3], Furkan BELLİBAŞ[4]

[1]Ar-Ge Personeli, BOLT Bağlantı Elemanları San. Tic. A.Ş., aslihan.kalyon@bolt.com.tr
[2]Ar-ge Müdürü, BOLT Bağlantı Elemanları San. Tic. A.Ş., alper.baygut@bolt.com.tr
[3]Ar-Ge Mühendisi, BOLT Bağlantı Elemanları San. Tic. A.Ş., yener.yilmaz@bolt.com.tr
[4]Ar-Ge Mühendisi, BOLT Bağlantı Elemanları San. Tic. A.Ş., furkan.bellibas@bolt.com.tr

Özet

Bağlantı elemanı üretimi için kullanılan yöntemlerden biri olan soğuk dövme prosesi, malzemenin plastik şekil değiştirme özelliğine dayalı olarak geliştirilen bir yöntemdir. Bu yöntem, bir tarafı sabit diğer tarafı hareketli kalıplar arasında, taşıyıcı pensler yardımıyla sonraki operasyona aktarılarak şekillendirmeye dayalıdır. Bu çalışmada; kafa altında kaynak punta formu (kaynak memesi) bulunan özel perçin üretimi için simülasyon destekli oluşturulan soğuk dövme tasarımları ile üretim çalışmalarını içermektedir. Bağlantı elemanı çeşitlerinden biri olan puntalı perçinler kullanıldığı yer itibariyle birden fazla parçayı birbirine montajlama görevi yapan ve uygulandığı yüzey ile bütünleşen bir ara elemandır. Çalışma kapsamında incelenen özel punta kaynaklı perçinin kritik sınır şartları bulunmaktadır. Çalışma konusu parçanın kritik özelliklerinin başında gelen altı adet puntaya sahip olmasının yanı sıra bu puntaları oluştururken punta çapı ve yüksekliğinin (Ø1.5 ±0.5 mm çap, 0.5 +0.3 mm yükseklik), puntalarda eş merkezliliğin (punta merkezleri arası uzaklık Ø14.5 mm) sağlanmış olup punta tasarım ölçülerinin istenen gerekliliklerin kapsamında elde edilmesi, aynı zamanda malzeme lif yönlenmelerinin homojen olması gerekmektedir. Parça geometrisi gereği fayda – maliyet değerlendirildiğinde hedeflere yönelik avantajlı olacak şekilde bir kalıp sabit - iki kalıp hareketli prensibi ile iki operasyonlu soğuk şekillendirme prosesi yapılmış, hazırlanan kalıp-operasyon tasarımları ile kurgulanan simülasyon analizleri incelenmiş ve prototip üretim gerçekleştirilmiştir. Belirtilen özelliklerin karşılanması adına taslak çizimde belirlenen, simülasyon sonrası oluşan ve prototip ürünün operasyon ölçüleri kıyaslanmış olup, %97 oranında tolerans değerlerini karşıladığı belirlenmiştir. Simülasyon destekli üretim çalışmaları ile sınır şartları elde edilmiş ve kalıp maliyetinde %20 azalma sağlanmıştır.

Anahtar kelimeler: Soğuk Dövme, Bağlantı Elemanı, Simülasyon

BUSBAR ENERJİ DAĞITIM SİSTEMİ ELEKTRİK SİMÜLASYONLARI

Ahmet Can YALÇIN[1], Mehmet Can BÜYÜKDÖĞERLİOĞLU[2], Hıdır GÖGÜLTER[3], Vedat VOŞKİ[4], Dursun ERİŞ[5], Tunahan İNAT[6], Ahmet FEYZİOĞLU[7]

[1]Eae Elektrik Asansör Endüstrisi İnşaat San. ve Tic. A.Ş., İstanbul, Türkiye, ahmetcan.yalcin@eaegroup.com
[2]Eae Elektrik Asansör Endüstrisi İnşaat San. ve Tic. A.Ş., İstanbul, Türkiye, mbuyukdogerlioglu@eaegroup.com
[3]Eae Elektrik Asansör Endüstrisi İnşaat San. ve Tic. A.Ş., İstanbul, Türkiye, hgogulter@eaegroup.com
[4]Eae Elektrik Asansör Endüstrisi İnşaat San. ve Tic. A.Ş., İstanbul, Türkiye, vvoski@eaegroup.com
[5]Eae Elektrik Asansör Endüstrisi İnşaat San. ve Tic. A.Ş., İstanbul, Türkiye, dursun.eris@eaegroup.com
[6]Eae Elektrik Asansör Endüstrisi İnşaat San. ve Tic. A.Ş., İstanbul, Türkiye, tunahan.inal@eaegroup.com
[7]Marmara Üniversitesi, Teknoloji Fakültesi, Makine Mühendisliği, İstanbul, Türkiye, ahmet.feyzioglu@marmara.edu.tr

Abstract

Lamine Busbar sistemleri, binlerce amperin dağıtıldığı günümüzün elektrik ve elektronik sistemleri için müşteriye özel tasarlanan üstün bir güç dağıtım sistemidir. Lamine Busbar, yalıtım malzemeler ile ayrılmış paralel iletken plakaların tek bir yapıda lamine edilmesiyle oluşur. Lamine Busbarlar özelleştirilebilir yapısı, kompakt tasarımı ile montaj kolaylığı ve dayanıklı bir yapı sunar. Bu yapısı sayesinde birçok alanda ihtiyaç duyduğunuz güvenilir ve modüler çözümler sunar. Geleneksel kablolama yöntemlerinde oluşabilecek kısmi deşarj ve dielektrik sorunlarını ortadan kaldırır.

Lamine Busbar tasarımı yapılırken farklı analiz yazılımları ile birçok olası en kötü durum senaryoları kurgulanıp yazılım platformunda simüle edilir. Bu sayede olası elektriksel arızalar ve güvenlik riskleri önceden tespit edilir, maliyetler ve riskler azaltılır, en optimum busbar modeli tasarlanır.

Bu çalışmada, Comsol Multiphysics yazılımı kullanılarak Lamine Busbar'ın çeşitli elektriksel simülasyonları gerçekleştirilmiştir. Optimizasyon çalışmaları yapılarak en uygun tasarım belirlenmiştir. Kısa devre anında Lamine Busbar'da oluşan maksimum sıcaklık ve termal etkisi, farklı izolasyon ve iletken türlerinde baranın davranışı, elektrik alan yoğunluğu analizi ve izolasyon malzemesi kalınlığının belirlenmesi, akım yoğunluğu analizi ve iletken kalınlığının belirlenmesi, farklı frekans aralıklarında skin effect ve manyetik alan etkisi gibi çeşitli simülasyonlar gerçekleştirilmiştir. GPO-3 malzemesinin termal strese karşı davranışı incelenmiştir. Endüktans kapasitans ve endüktif reaktans değerleri bulunarak baraya etkisi anlatılmıştır.

Keywords: Comsol Multiphysics, Busbar, Simülasyon

12.07.2024

ISBN: 978-625-94809-5-4

ASES PUBLICATIONS – 2024©